Article

Developmental Cell

E2F-Family Members Engage the PIDDosome to Limit Hepatocyte Ploidy in Liver Development and Regeneration

Graphical Abstract

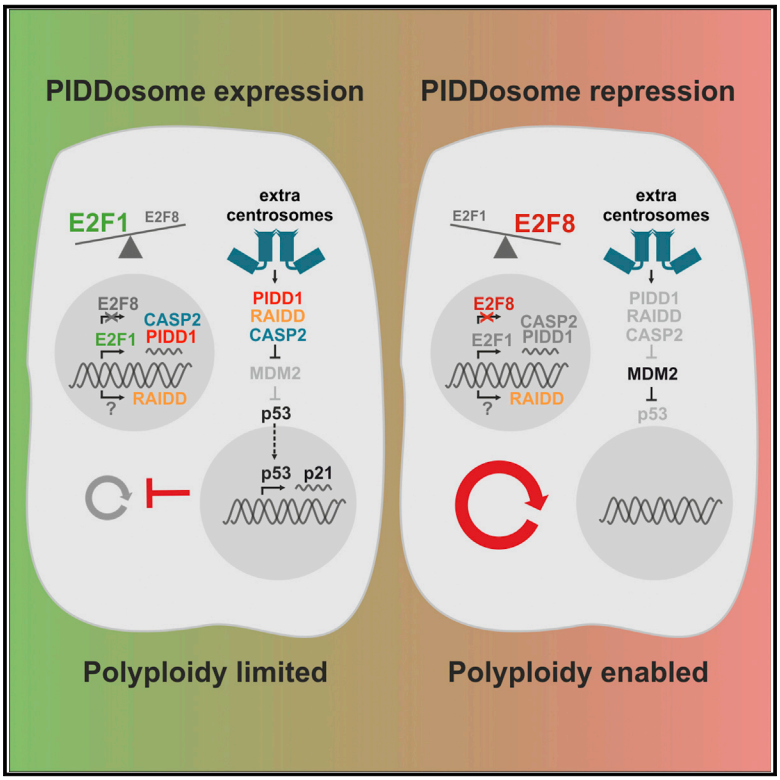

Highlights

- The PIDDosome controls hepatocyte ploidy during postnatal development & regeneration
- The PIDDosome defines the speed of liver regeneration posthepatectomy
- Aneuploidy in the liver correlates with basal ploidy state but is not limited by CASP2
- E2F family members regulate expression of CASP2 and PIDD1 for liver ploidy control

Authors

Valentina C. Sladky, Katja Knapp, Claudia Soratroi, ..., Floris Foijer, Alain de Bruin, Andreas Villunger

Correspondence

andreas.villunger@i-med.ac.at

In Brief

Sladky et al. report a key role for the PIDDosome in regulating p53 activation to limit hepatocyte polyploidy during juvenile liver growth and regeneration. Expression of essential PIDDosome components is controlled by a E2F-family regulated circuitry. The study defines the PIDDosome as a putative target to enhance liver regeneration.

Sladky et al., 2020, Developmental Cell *52*, 335–349
February 10, 2020
https://doi.org/10.1016/j.devcel.2019.12.016

CellPress

Developmental Cell
Article

E2F-Family Members Engage the PIDDosome to Limit Hepatocyte Ploidy in Liver Development and Regeneration

Valentina C. Sladky,[1] Katja Knapp,[1] Claudia Soratroi,[1] Julia Heppke,[1] Felix Eichin,[1] Lourdes Rocamora-Reverte,[1] Tamas G. Szabo,[1] Laura Bongiovanni,[2] Bart Westendorp,[2] Eva Moreno,[2] Elsbeth A. van Liere,[2] Bjorn Bakker,[3] Diana C.J. Spierings,[3] René Wardenaar,[3] David Pereyra,[4] Patrick Starlinger,[4] Simon Schultze,[5] Michael Trauner,[5] Tatjana Stojakovic,[6] Hubert Scharnagl,[6] Luca L. Fava,[7] Floris Foijer,[3] Alain de Bruin,[2,8] and Andreas Villunger[1,9,10,11,*]

[1]Division of Developmental Immunology, Biocenter, Medical University of Innsbruck, 6020 Innsbruck, Austria
[2]Department of Pathobiology, Faculty of Veterinary Medicine, Utrecht University, 3584 CL Utrecht, the Netherlands
[3]European Research Institute for the Biology of Ageing, University of Groningen, University Medical Center Groningen, 9713 AV Groningen, the Netherlands
[4]Department of Surgery, Medical University of Vienna, General Hospital, 1090 Vienna, Austria
[5]Department of Internal Medicine III, Division of Gastroenterology and Hepatology, Medical University of Vienna, 1090 Vienna, Austria
[6]Medical University of Graz, Clinical Institute of Medical and Chemical Laboratory Diagnostics, 8010 Graz, Austria
[7]Armenise-Harvard Laboratory of Cell Division, Department of Cellular, Computational and Integrative Biology - CIBIO, University of Trento, 38123 Povo, Italy
[8]Department of Pediatrics, University Medical Center Groningen, University of Groningen, 9713 AV Groningen, the Netherlands
[9]Ludwig Boltzmann Institute for Rare and Undiagnosed Diseases, 1090 Vienna, Austria
[10]CeMM Research Center for Molecular Medicine of the Austrian Academy of Sciences, 1090 Vienna, Austria
[11]Lead Contact
*Correspondence: andreas.villunger@i-med.ac.at
https://doi.org/10.1016/j.devcel.2019.12.016

SUMMARY

E2F transcription factors control the cytokinesis machinery and thereby ploidy in hepatocytes. If or how these proteins limit proliferation of polyploid cells with extra centrosomes remains unknown. Here, we show that the PIDDosome, a signaling platform essential for caspase-2-activation, limits hepatocyte ploidy and is instructed by the E2F network to control p53 in the developing as well as regenerating liver. *Casp2* and *Pidd1* act as direct transcriptional targets of E2F1 and its antagonists, E2F7 and E2F8, that together co-regulate PIDDosome expression during juvenile liver growth and regeneration. Of note, whereas hepatocyte aneuploidy correlates with the basal ploidy state, the degree of aneuploidy itself is not limited by PIDDosome-dependent p53 activation. Finally, we provide evidence that the same signaling network is engaged to control ploidy in the human liver after resection. Our study defines the PIDDosome as a primary target to manipulate hepatocyte ploidy and proliferation rates in the regenerating liver.

INTRODUCTION

Polyploidization, the balanced amplification of the whole genome, is commonly observed in plants, insects, and fungi, as well as in some vertebrates, including frogs and fish (Gjelsvik et al., 2019; Otto, 2007). In contrast, mammalian cells are mainly diploid, and polyploidy is noted as a potential danger facilitating chromosomal instability (CIN) and thereby transformation (Holland and Cleveland, 2009). Thus, polyploidy is limited to certain tissues and cell types where it is considered beneficial for the execution of organ-specific functions, such as protection of the urothelium, muscle cell contraction, platelet shedding or, counterintuitively, the protection from liver cancer (Abmayr and Pavlath, 2012; Pang et al., 2005; Wang et al., 2018; Zhang et al., 2018a). Remarkably, the generation of polyploid cells during organogenesis frequently involves incomplete cytokinesis (Lens and Medema, 2019; Pandit et al., 2013). In the rodent liver, physiological polyploidization starts at the time of weaning when diploid hepatocytes fail to complete cytokinesis and generate binucleated, tetraploid progeny. Following this first wave of polyploidization, hepatocytes either divide normally to generate mononucleated tetraploid cells or fail cytokinesis again to become octaploid (Celton-Morizur et al., 2009; Margall-Ducos et al., 2007). Yet, polyploid cell divisions with clustered centrosomes or multipolar mitoses are prone to segregation errors generating CIN and aneuploid progeny, which is often detrimental even for cancer cells (Holland and Cleveland, 2009; Tang and Amon, 2013). In the liver, however, this has not been formally demonstrated *in vivo* but aneuploidy was proposed to be beneficial by providing genetic diversity posing an advantage in adaption to various stressors or injury and is also frequently observed in hepatocellular carcinoma (Cancer Genome Atlas Research Network, 2017; Duncan et al., 2012a). This suggests a certain trade-off between fast adaptation to hepatotoxic stress and increased cancer risk. The actual degree of aneuploidy in the liver, however, remains a matter of debate (Duncan et al., 2010, 2012b; Knouse et al., 2014, 2018).

Hepatocyte polyploidization is a well-organized process best studied in mice where its onset during weaning is controlled by increases in insulin levels (Celton-Morizur et al., 2009; Margall-Ducos et al., 2007). Moreover, hepatocyte ploidy is regulated by members of the E2F family of transcription factors, which control expression of key proteins required for cell cycle progression and cytokinesis (Chen et al., 2012; Conner et al., 2003; Pandit et al., 2012). While the transcriptional activator E2F1 promotes normal cell division, the atypical, partially redundant E2F family members, E2F7 and E2F8, repress transcription of several cytokinesis effectors such as *ECT2*, *MKLP1*, or *RACGAP* and thereby facilitate cytokinesis failure. Consistently, overexpression of E2F1 or liver-specific co-deletion of E2F7 and E2F8 prevents weaning-induced polyploidization. As a consequence, hepatocytes in these mice are largely diploid (Chen et al., 2012; Conner et al., 2003; Pandit et al., 2012). In contrast, ablation of E2F1 results in an even further increase of hepatocyte ploidy (Chen et al., 2012; Pandit et al., 2012). Whereas the physiological relevance of increased ploidy for liver function remains unclear, recent evidence suggests that it protects from tumorigenesis, presumably by providing a reservoir of tumor suppressors in hepatocytes (Kent et al., 2016; Zhang et al., 2018a, 2018b). The exact molecular basis limiting natural polyploidization in the adult or regenerating liver, however, remains to be defined. A well-established player in this process is p53, shown to limit liver ploidy during development and regeneration (Kurinna et al., 2013). How p53 becomes activated in hepatocytes to restrict polyploidy in organogenesis or tissue repair remains unclear.

Caspase-2 is a member of the caspase family of endopeptidases, which are best known for their functions in cell death and inflammation (McIlwain et al., 2013). Caspase-2 contains a caspase activation and recruitment domain (CARD) required for activation (Bouchier-Hayes and Green, 2012; Kumar, 2009). As such, caspase-2 is structurally similar to the initiator caspases-1, -4, -5, and -9 that become activated in inflammasomes or the apoptosome, respectively (McIlwain et al., 2013). The protein complex needed for caspase-2 activation was dubbed the PIDDosome and is formed by PIDD1 and RAIDD/CRADD that assemble into an activation platform for caspase-2 (Tinel and Tschopp, 2004). Initially described to be a cell-death mediator and p53 effector in the DNA damage response, the relevance of the PIDDosome in health and disease remained uncertain (Fava et al., 2012; Manzl et al., 2009; Sladky et al., 2017; Tinel and Tschopp, 2004).

We recently provided firm evidence that the PIDDosome acts upstream of p53 as a sensor for supernumerary centrosomes (Fava et al., 2017). Extra centrosomes occur either due to aberrant centrosome amplification or during an incomplete cell cycle, as centriole biogenesis is tightly coupled to DNA replication in S phase. Abortive cell-cycle modalities such as endomitosis, endoreduplication, or incomplete cytokinesis are associated with centrosome amplification (Nigg and Holland, 2018; Tachibana et al., 2005). Accumulation of extra centrosomes alerts PIDD1, residing at the mother centriole, to kick-start a signaling cascade, which arrests the cell cycle (Fava et al., 2017). PIDDosome assembly activates caspase-2, which cleaves MDM2 at Asp^{367} removing the RING domain and killing its E3 ligase activity. This leads to p53 stabilization, p21 induction, and subsequent cell-cycle arrest (Fava et al., 2017; Oliver et al., 2011). Of note, supernumerary centrosomes seem to exclusively rely on caspase-2 for p53 activation (Fava et al., 2017). Consistently, caspase-2-deficient mice show increased hepatocyte ploidy comparable to that found in $p53^{-/-}$ animals, and double-deficiency in caspase-2 and p53 did not cause an additional ploidy increase in support of their epistatic relation (Fava et al., 2017).

Here, we set out to dissect the role of the PIDDosome in liver development and regeneration and addressed the question if aberrant increases in polyploidy can promote aneuploidy in the liver.

RESULTS

The PIDDosome-p53 Axis Regulates Hepatic Ploidy during Postnatal Liver Development

To analyze the role of the PIDDosome in liver ploidy, we used flow cytometry to determine the DNA content of hepatocytes isolated from adult mice. We found that hepatocytes lacking any one of the three PIDDosome components showed increased ploidy, comparable to those isolated from livers of $p53^{-/-}$ or $p21^{-/-}$ mice (Figure 1A), confirming previous results (Fava et al., 2017; Kurinna et al., 2013; Sheahan et al., 2004). All mouse mutants tested showed an on average 30% higher mean DNA content, depicted as weighted mean ploidy (Figure 1A).

Next, we investigated the timing of PIDDosome activation during developmental hepatocyte polyploidization. In order to synchronize this process, mice were weaned at the age of 20 days and DNA content was analyzed either before (day 20) or after separation from their mothers (days 22, 25, and 28). Regardless of the genotype tested, the majority of hepatocytes were found to be diploid before (day 20) and shortly after weaning (day 22). Five days post-weaning, however, most hepatocytes had undergone at least one round of cell division and incomplete cytokinesis (Figure 1B). Importantly, in WT hepatocytes, this coincided with the loss of the pro-form of caspase-2, indicating its autoproteolytic activation (Butt et al., 1998), as well as with p53 induction (Figures 1C and S1A). In contrast, caspase-2-deficient hepatocytes failed to activate p53 and showed a significant increase in mean ploidy over time, most pronounced on day 28 (Figures 1B and S1A). Of note, at this point of analysis, p53 returned to basal levels (Figure S1A). p53 activation after weaning was strictly PIDDosome-dependent (Figure 1C). Consistently, PIDDosome deficiency results in enhanced polyploidization mirroring the one noted in $p53^{-/-}$ or $p21^{-/-}$ mice (Figures 1A and 1C). Together, these data show that p53 is engaged by the PIDDosome to limit excessive hepatocyte polyploidization.

Surprisingly, hepatic ploidy continuously increased with age in WT and PIDDosome-deficient mice alike (Figure 1D), suggesting only transient action of the PIDDosome at the time of weaning. Thus, we analyzed the levels of the PIDDosome mRNA and/or protein, during postnatal liver development and found that indeed *Casp2*, *Pidd1*, and *Raidd* transcript levels declined with increasing ploidy and age (Figure 1F). RAIDD protein levels, however, remained stable over time, whereas the pro-form of caspase-2 did not re-accumulate following

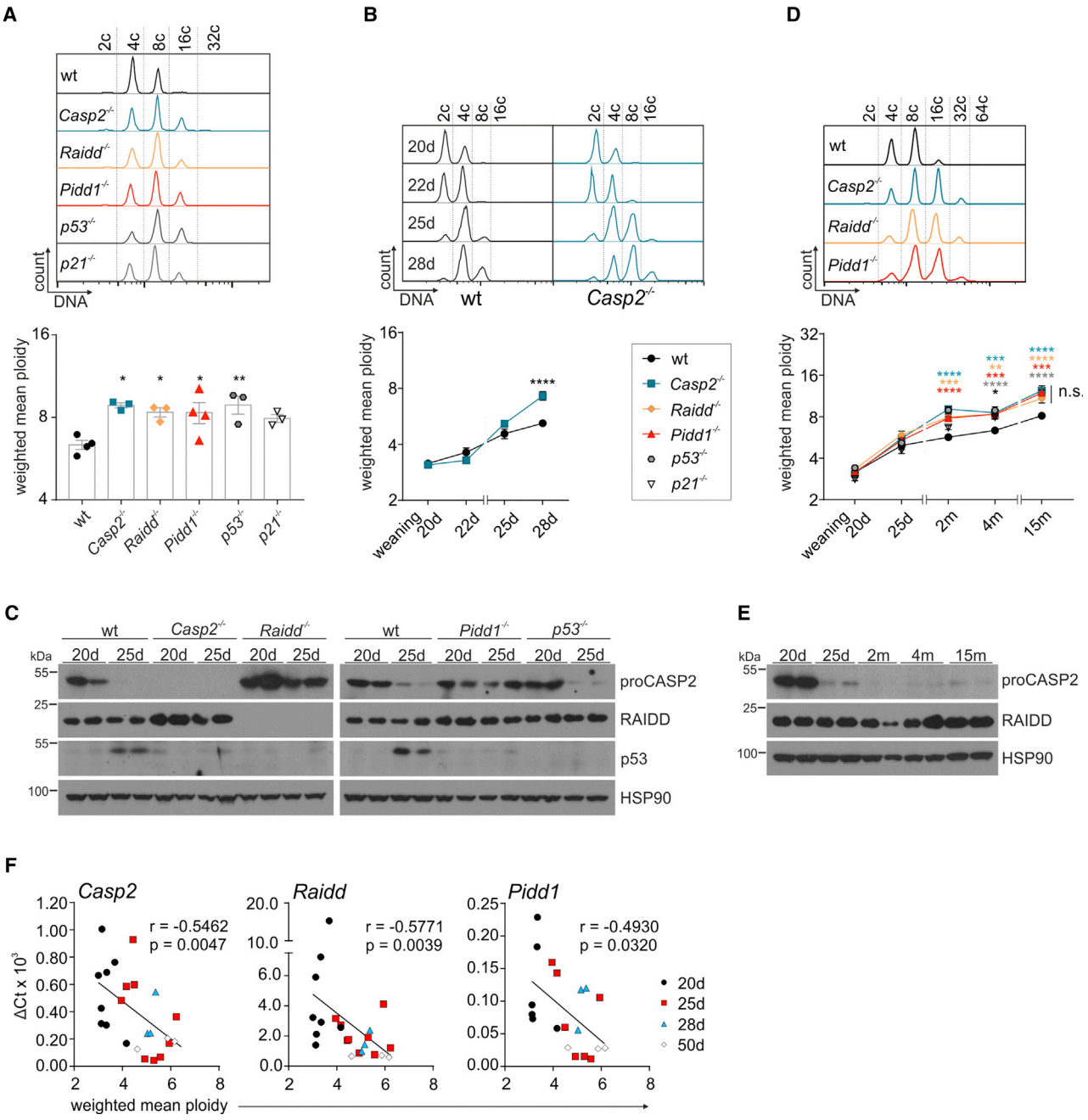

Figure 1. The PIDDosome-p53 Axis Regulates Hepatic Ploidy during Postnatal Liver Development

(A) Representative histograms and weighted mean ploidy quantification of hepatocytes isolated from 12- to 14-week-old male mice of the indicated genotypes. The formula used can be found in the statistics section. Hepatocytes were fixed and stained with propidium iodide to analyze DNA content by flow cytometry (n = 3–8 per time point; detailed mouse numbers are shown in Table S7).

(B) Representative histograms and weighted mean ploidy of isolated hepatocytes from WT and *Casp2*$^{-/-}$ mice before and after timed weaning at day 20 (n = 3–8).

(C) Analysis of CASP2, RAIDD, and p53 protein in hepatocytes isolated from mice of the indicated genotypes, before (20 days), and 5 days after weaning (25 days). (D) Representative histograms of WT and PIDDosome-deficient hepatocytes at the age of 15 months and weighted mean ploidy analyzed over time. *p53*$^{-/-}$ and *p21*$^{-/-}$ hepatocytes were analyzed at 20 days, 25 days, 2 months, and 4 months (n = 3–8).

(E) Time-course analysis of caspase-2 and RAIDD protein levels in WT hepatocytes.

(F) PIDDosome mRNA levels were assessed in isolated hepatocytes by qRT-PCR before and at indicated time points after weaning. Data were analyzed with respect to the weighted mean ploidy. Transcript levels negatively correlate with increasing ploidy as reflected by Spearman's correlation coefficient (linear regression: *Casp2* r^2 = 0.3158, p = 0.0035; *Raidd* r^2 = 0.1766, p = 0.0458; *Pidd1* r^2 = 0.2735, p = 0.0216). Mean ± SEM; *p < 0.05, **p < 0.01, ***p < 0.001, ****p < 0.0001.

PIDDosome-dependent autoproteolytic activation at the time of weaning (Figure 1E). Mouse PIDD1 protein expression was not detectable by western blotting with commercially available antibodies in hepatocyte extracts. The transcriptional downregulation of *Casp2* and *Pidd1* coincides with further polyploidization (Figures 1D and 1E), indicating that developmental inactivation of the PIDDosome is required to facilitate homeostatic proliferation of polyploid hepatocytes in the presence of extra centrosomes. Remarkably, increased liver ploidy in PIDDosome mutant mice had no or only marginal effects on liver function, based on the analysis of ALT, AST, bilirubin, urea, cholesterol, and triglycerides in sera of 4- or 15-month-old mice (Figure S1B).

The PIDDosome Restricts Polyploidization during Liver Regeneration

Hepatocytes in the regenerating liver can abort cytokinesis and p53 controls the extent of ploidy increase in this setting (Kurinna et al., 2013; Sigal et al., 1999). Despite the noted downregulation of *Casp2* and *Pidd1* after weaning, we wondered if the PIDDosome is still involved in ploidy control in the adult liver or if p53 is activated by alternative routes during regeneration. In order to test this, we performed 68% partial hepatectomy (PH) on 12–14-week-old mice of different genotypes and analyzed recovery of liver mass as well as hepatocyte ploidy. In line with previous reports, polyploidy increased during regeneration and peaked between 48 and 72 h post-resection in a p53-dependent manner (Kurinna et al., 2013; Sigal et al., 1999; Wilkinson et al., 2018) (Figures 2A–2C and S2A). Intriguingly, PIDDosome-deficient cells showed a polyploidization pattern similar to $p53^{-/-}$ hepatocytes (Figure 2C). Albeit starting from a different baseline, the overall increase in ploidy was again significantly higher compared to that seen in WT controls (Figures 2A–2C). Seven days post-PH, PIDDosome-deficient, as well as $p53^{-/-}$ livers, reached an at least 2-fold higher increase in mean ploidy, compared with livers from WT mice (Figures 2B and 2C). Whereas the weighted mean DNA content per cell increased on average by 18% in the WT, the increase observed in PIDDosome- or p53-deficient livers ranged from 50% to 90% after 7 days of regeneration (Figure 2B). Histopathological analysis of liver sections confirmed differences in cell size and frequency of binucleation (Figures 2F–2I). Moreover, the peak in ploidy was observed at 96 h in the absence of the PIDDosome, whereas the mean ploidy of WT hepatocytes began to decline already after 72 h, indicating altered proliferation dynamics (Figures 2A and 2C). Strikingly, $Casp2^{-/-}$ livers showed a prolonged proliferation phase, reflected by a higher mitotic index (Figures 2D, 2F, and S2B). Moreover, the significantly increased relative liver weight (LW/BW) 72 h post-resection clearly shows accelerated regeneration of $Casp2^{-/-}$ livers (Figures 2D–2F). Yet, 7 days post-resection, both WT and $Casp2^{-/-}$ animals have recovered their original liver mass. Similarly, albeit transiently increased ALT levels at 48 h in PIDDosome-deficient mice, liver integrity and function were similar between genotypes after 7 days, as indicated by comparable serum levels of liver enzymes, lipids, bilirubin, and urea (Figures 2D and S2C). These findings document that the PIDDosome limits the degree of polyploidization and the kinetics of liver regeneration.

Aneuploidy in the Liver Increases with Ploidy but Is Not Limited by Caspase-2

Caspase-2 was proposed to be required for the clearance of aneuploid tumor cells and low expression levels were shown to facilitate aneuploidy tolerance in colorectal cancer patients (Dawar et al., 2016; López-García et al., 2017). Consistent with massively increased polyploidization, $Casp2^{-/-}$ livers frequently showed multipolar mitoses and multinucleation in histological sections, suggesting less proficient chromosome segregation during regeneration that may drive aneuploidy (Figures 3A–3C and S2A).

To analyze chromosomal stability, we performed single-cell sequencing of WT and $Casp2^{-/-}$ hepatocytes. Cells were isolated either before or 7 days after PH when regeneration is completed. Based on their DNA content, hepatocyte nuclei were sorted, and 48 cells of each ploidy state and genotype were subjected to low-coverage whole genome sequencing, as described by Bakker et al. (2016). This analysis revealed that only a very low fraction of hepatocytes were indeed aneuploid, displaying either whole chromosome or structural alterations (Figures 3D–3F and S3A). The degree of aneuploidy clearly increased with the basal level of polyploidy but was independent of the genotype analyzed (Figures 3D–3F and S3A). Forcing polyploid cells into proliferation during liver regeneration did not lead to a considerable increase in aneuploidy. However, we observed a higher degree of copy number variations in the octaploid fraction of regenerated $Casp2^{-/-}$ hepatocytes (Figure 3E). As this occurred in the absence of notable cell death (Figure S3D), we conclude that the increased level of aneuploidy seen is most likely a secondary consequence of multipolar mitoses, as about 1% of caspase-2 deficient hepatocytes harbor more than two nuclei at the time of analysis (Figure 3C). These data suggest that caspase-2 is not directly involved, arguing against a role in deleting aneuploid cells, at least in the healthy or regenerating liver. However, caspase-2 impacts aneuploidy by restricting the degree of basal ploidy levels in the liver.

Proliferating Adult Hepatocytes Engage the PIDDosome-p53-p21 Axis to Restrict Polyploidization

Given the noted downregulation of the PIDDosome after weaning and the differences in polyploidy after PH, we analyzed mRNA and protein expression of all PIDDosome components during regeneration. We found strong induction of *Casp2* and *Pidd1* mRNA, as well as caspase-2 protein, during liver regeneration. Reminiscent of post-weaning development, *Raidd* mRNA and protein were unchanged. *Casp2* and *Pidd1 mRNA* levels peaked at 48 h post-PH suggesting a link between expression levels and proliferation. At the same time p53 was stabilized in a PIDDosome-dependent manner (Figures 4A and 4B). Along with it, *p21* expression was strongly induced in WT hepatocytes whereas *p21* mRNA levels were significantly lower in PIDDosome- and p53-deficient cells (Figures 3A and 3C). Since the PIDDosome is activated by extra centrosomes, we reasoned that p21 would be preferentially induced in polyploid hepatocytes. Using IHC, we correlated p21 protein levels with cell size. Indeed, 72 h post-resection, p21 protein was predominantly induced in polyploid cells,

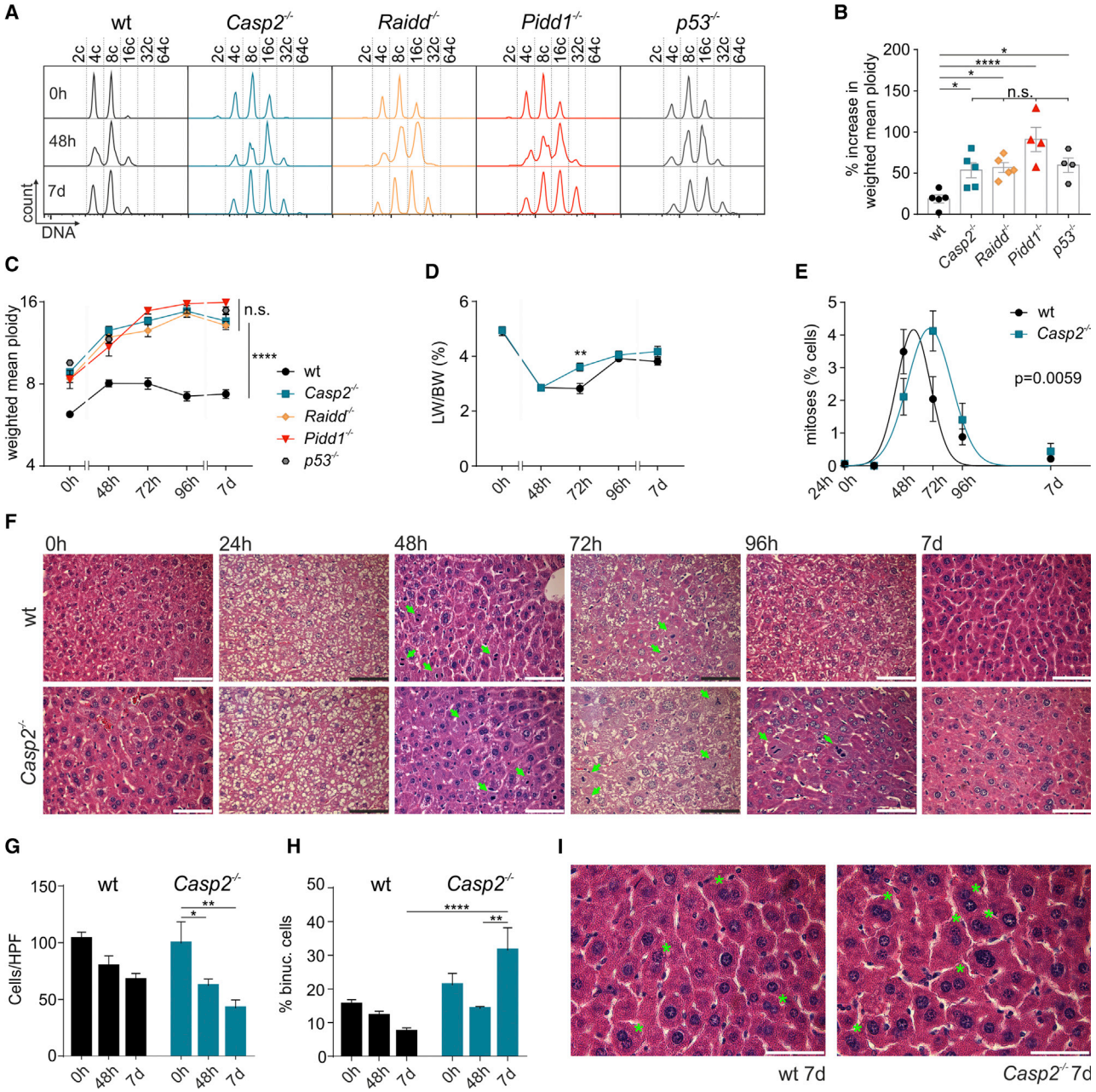

Figure 2. The PIDDosome Restricts Polyploidization during Liver Regeneration

(A) Representative histograms showing the DNA content of hepatocytes isolated at an age of 14 weeks before (0 h) or 48 h and 7 days after PH.

(B) Percentage of relative increase in weighted mean ploidy after 7-day regeneration.

(C) Weighted mean ploidy of hepatocytes at the indicated time points before and after PH. Data for mice before PH (0 h) are the same as displayed in Figure 1A.

(D) Analysis of liver weight to body weight (LW/BW) ratios of WT and *Casp2*$^{-/-}$ mice during regeneration.

(E and F) Mitotic index of WT and Casp2 $^{-/-}$ livers during regeneration was assessed by counting mitotic figures in H&E-stained liver sections shown in (F). Green arrows indicate mitotic hepatocytes.

(G and H) Number of WT and *Casp2*$^{-/-}$ hepatocytes per 40× high power field (HPF) and (H) percentage of binucleated cells before (0 h) and 48 h or 7 days after PH.

(I) Representative images (80×) showing binucleation 7 days after PH. Green asterisks mark binucleated cells. Scale bars represent 100 μm; n = 3–9 (Table S7); mean ± SEM; *p < 0.05, **p < 0.01, ***p < 0.001, ****p < 0.0001.

defined as binucleated cells and hepatocytes containing nuclei with twice the diameter of those of pericentral, presumably diploid, hepatocytes (Figures 4D and 4E). In contrast, p21 levels were significantly lower in Casp2$^{-/-}$ livers and showed no difference between ploidy states. Together, these data demonstrate that hepatocytes reactivate the PIDDosome to limit proliferation rates after cell cycle re-entry in a polyploid state (Figures 2D, 2E, and 4E).

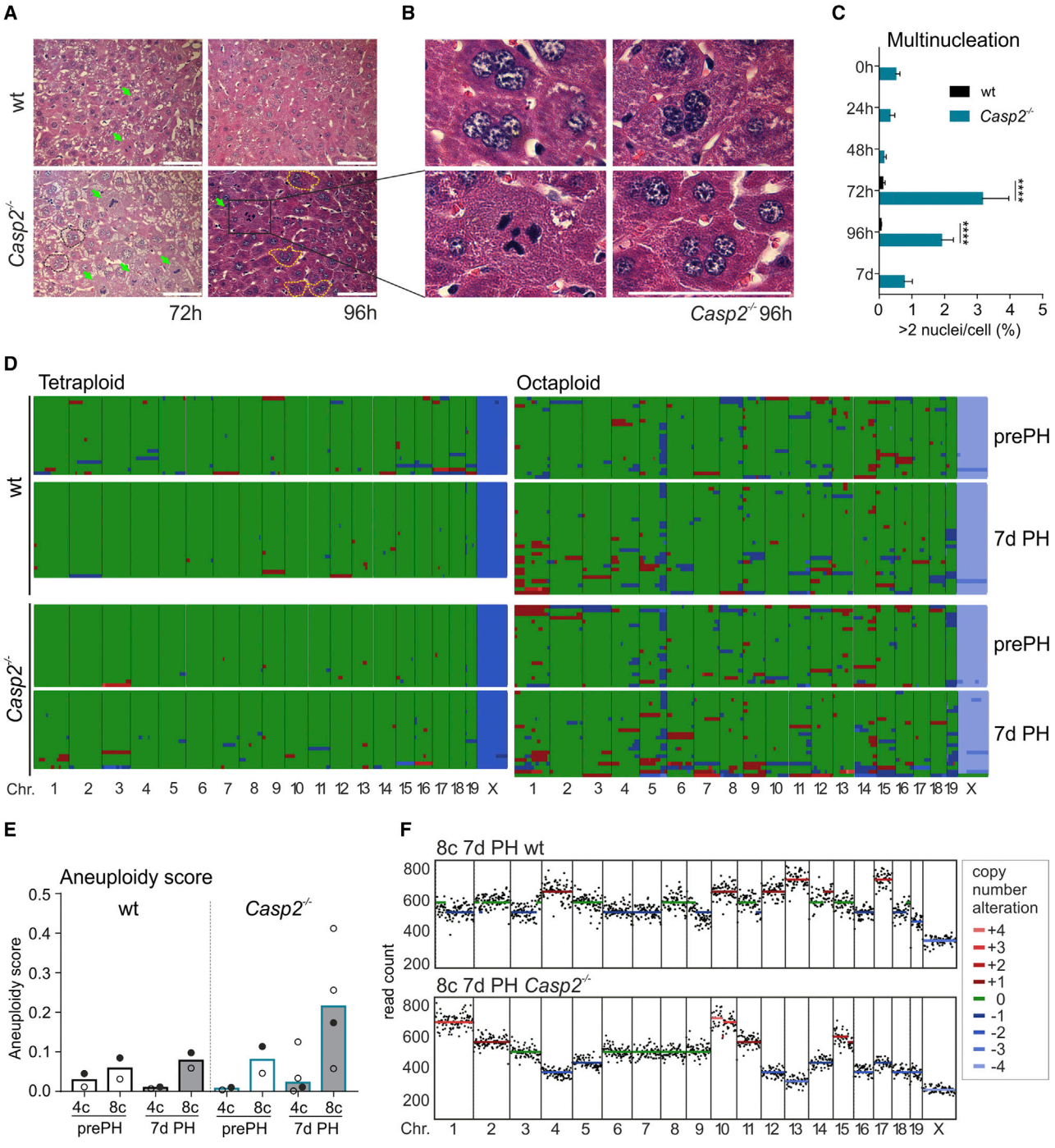

Figure 3. Aneuploidy in the Liver Increases with Overall Ploidy but Is Not Limited by Caspase-2

(A) H&E stained liver sections at 72 and 96 h post-PH of WT and *Casp2*$^{-/-}$ mice. Dashed lines mark cells with multiple nuclei and green arrows indicate mitotic hepatocytes.

(B) Examples of aberrant mitoses and cells with >2 nuclei in *Casp2*$^{-/-}$ liver 96 h post-PH.

(C) Quantification of multinucleation (cells with >2 nuclei) during liver regeneration in WT and *Casp2*$^{-/-}$ mice. n = 3–8 (Table S7), scale bars represent 100 μm; mean ± SEM; ****p < 0.0001.

(D) Genome-wide heatmaps showing copy number variation (CNV) found in WT and *Casp2*$^{-/-}$ hepatocytes. 48 nuclei of n = 2–4 mice were sequenced per condition. Non-robust or erroneous libraries were excluded by two-step quality control.

(legend continued on next page)

Human Hepatocytes Engage the PIDDosome during Liver Regeneration

To explore conservation of mechanism, we first made use of the human hepatocellular carcinoma cell line, HepG2. In accordance with previous experiments in human A549 lung adenocarcinoma cells (Fava et al., 2017), perturbing cytokinesis using the AuroraB kinase inhibitor, ZM447439, resulted in PIDDosome-dependent and caspase-2-directed proteolysis of MDM2 and p53 stabilization (Figure 5A). Upon loss of either PIDDosome component, cleavage of MDM2 was abrogated and p53 levels were strongly reduced (Figure 5A). This confirms that the PIDDosome can control p53 in response to cytokinesis failure in human hepatocytes.

To provide first evidence that the PIDDosome may also be relevant for ploidy control in primary hepatocytes, we next tested whether its regulation can be observed during liver regeneration. We isolated RNA from patients undergoing liver surgery according to the ALPPS (associating liver partition and portal vein ligation for staged hepatectomy) procedure. Thereby, the regenerative capacity of the liver is exploited to allow resection of hepatic tumors or liver-metastases, which cannot be removed by standard staged resection (Schnitzbauer et al., 2012). During the first surgery, ligation of the portal vein and *in situ* splitting of one liver lobe induces enhanced proliferation in the other liver lobe. The split lobe is then removed in a second surgery 5–15 days later. Tissue biopsies of healthy liver, sampled from the regenerating lobe during the first and second surgery of five patients diagnosed with metastatic colorectal carcinoma undergoing the ALPPS procedure, were analyzed (clinical data shown in Table S1).

Recapitulating our results in mice and in line with previous observations, hepatocyte ploidy increased during regeneration (Figures 5B and 5C) (Schnitzbauer et al., 2012). We assessed mRNA levels of *E2F1* and *CCNA2* (Cyclin A2) and found that hepatocytes of four out of five patients actively proliferate, indicating ongoing liver regeneration. Strikingly, *p21* mRNA levels were found generally increased in the regenerating livers, which coincided with an at least 2.5-fold induction of *CASP2* mRNA, seen in four out of five patient samples (Figure 5D). Patient #2 who failed to induce *CASP2* mRNA did also not show signs of proliferation, as reflected by reduced *E2F1* and steady *CCNA2* expression. Of note, this patient also presented with liver dysfunction after both surgeries (Figure 5D; Table S1). *PIDD1* mRNA expression, was found to only mildly increase in 4/5 samples analyzed while *RAIDD* mRNA levels differed strongly between patients (Figure S4A), indicating the need for more detailed follow up studies on larger patient cohorts to time-resolve their regulation dynamics. However, considering the time between biopsy sampling in the different patients for a pseudo time-course analysis, *CCNA2* and *p21* induction followed a similar behavior, as observed during murine liver regeneration (Figure 5E). Taken all together, these data suggest that the PIDDosome contributes to *p21* mRNA induction in the regenerating human liver to prevent excessive polyploidization during regeneration.

An E2F Regulatory Circuit Instructs PIDDosome Expression and Function in Hepatocytes

The above described data indicate that expression of *CASP2* and *PIDD1* in hepatocytes is coupled to proliferation during development and regeneration. To gain first information on the transcriptional control of the PIDDosome, we analyzed genes co-expressed with *CASP2*, *PIDD1,* and *RAIDD* that we retrieved from the STRING database (Szklarczyk et al., 2019). For *CASP2* and *PIDD1* the associated hallmark gene sets and GO terms mainly included pathways related to proliferation. Strikingly, the highest significance and overlap was found with genes of the hallmark pathways "G2/M checkpoint" and "E2F targets" (Figures 6A, S5A, and S5B). Next, we also analyzed the MSigDB transcription factor target data set, which includes information on putative transcription factor binding motifs. Genes co-expressed with *CASP2* and *PIDD1* were mostly E2F targets (Figure 6B). In contrast, no significant results were found for *RAIDD*. Of note, E2F transcription factor family members are crucial for hepatocyte polyploidization (Chen et al., 2012; Conner et al., 2003; Pandit et al., 2012) and showed an expression pattern similar to *CASP2* and *PIDD1* during liver development and regeneration (Figure 6C).

Intriguingly, sequence analysis of the murine and human *CASP2*, *PIDD1*, and *RAIDD/CRADD* promoter regions revealed that their 5′UTRs contain canonical E2F binding motifs (Figure 6D). Hence, we analyzed available ChIP-seq data sets for promoter occupancy with E2F1, E2F7, and E2F8. Both replicates of the ENCODE HeLaS3 cell samples showed strongly enriched E2F1 peaks near the transcription start sites (TSS) of *CASP2* and *PIDD1* (Figures 6D and S5C; Tables S2 and S3). E2F7 and E2F8 were also both significantly enriched at the *CASP2* promoter (Figure 6D; Tables S4 and S5). No E2F7 or E2F8 peaks could be called for the *PIDD1* proximal promoter, although visual inspection suggested some enrichment at the same genomic position near the *PIDD1* TSS as the E2F1 peak (Figure 6D). In contrast, none of these transcription factors were found in the *RAIDD* promoter region. Analysis of data sets of an additional experiment, performed in primary mouse hepatocytes overexpressing human E2F1, confirmed these results showing a 3.71- and 23.38-fold enrichment in the TSS of *Casp2* and *Pidd1*, respectively (GEO GSE74006) (Denechaud et al., 2016) (Figure 5C).

To validate these results experimentally, we manipulated expression levels of the respective E2F family members and assessed the levels of *CASP2*, *PIDD1,* and *RAIDD/CRADD* expression. Doxycycline-induced overexpression of E2F7 or E2F8 in RPE1 cells significantly reduced *CASP2* transcript levels. Again, no effect was observed on *RAIDD* mRNA but expression of *PIDD1* was reduced upon E2F8 induction. Repression of *CCNE1* by E2F7 or E2F8 served as an internal control (Figure 7A). Transcriptional repression by E2F7 or E2F8 also resulted in decreased caspase-2 protein levels while neither RAIDD nor PIDD1 showed a substantial reduction at the time of analysis

(E) Aneuploidy scores for each genotype, time point, and ploidy state show increasing CNV in octaploid samples. Robustly sequenced nuclei per condition: WT prePH (4c) = 34, WT prePH (8c) = 35, WT 7 days PH (4c) = 49, WT 7 days PH (8c) = 50, *Casp2*$^{-/-}$ prePH (4c) = 39, *Casp2*$^{-/-}$ prePH (8c) = 35, *Casp2*$^{-/-}$ 7 days PH (4c) = 75, and *Casp2*$^{-/-}$ 7 days PH (8c) = 75. Black dots mark samples shown in (D), data are represented as median.

(F) Single-cell plots from cells isolated after PH from WT and *Casp2*$^{-/-}$ livers with a basal ploidy of 8c showing a high degree of whole chromosome and structural CNV. All single-cell plots are deposited in Mendeley Data (https://data.mendeley.com/datasets/vfpgvhcvh5/1).

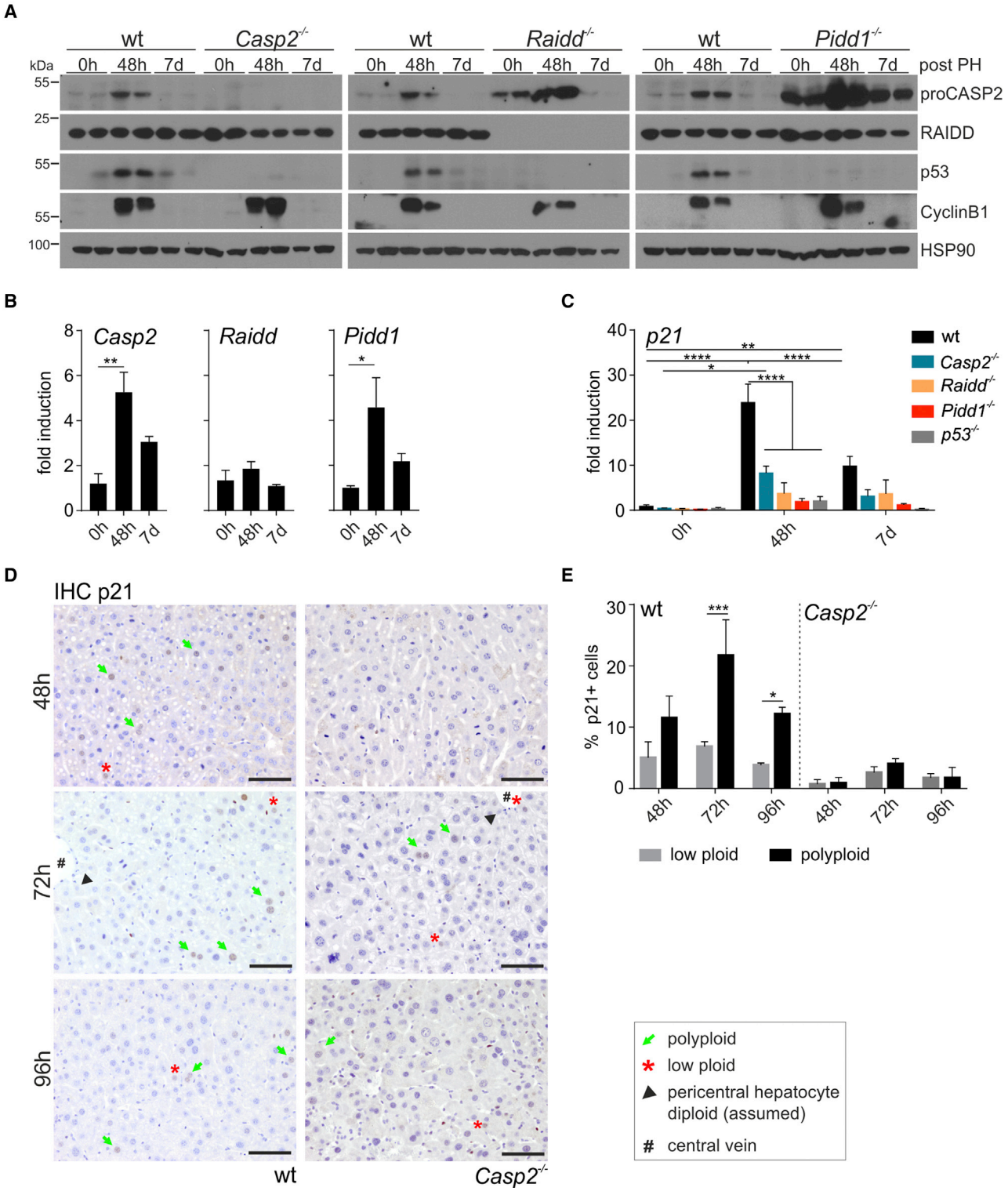

Figure 4. Adult Hepatocytes Induce and Activate the PIDDosome-p53-p21 Axis to Restrict Excessive Polyploidization during Regeneration

(A) Immunoblot analysis assessing CASP2, RAIDD, p53, and cyclin B1 expression in hepatocytes isolated from 14-week-old mice (0 h) before and 48 h and 7 days after PH.

(B) Transcript levels of *Casp2*, *Raidd*, and *Pidd1* in isolated hepatocytes also shown in (A).

(legend continued on next page)

(Figures 7B and S6A). Transient overexpression of E2F1 in HepG2 cells resulted in marked increases in *CASP2* and *PIDD1* mRNA, but this finding was hard to reproduce by immunoblotting (Figure 7C, data not shown), potentially because E2F1 also increases levels of E2F7 and E2F8, which in turn repress caspase-2 in a negative feedback loop (Chen et al., 2009). Encouragingly, *Casp2* transcript and protein levels were found to be higher in liver extracts from *E2f7*$^{-/-}$*E2f8*$^{-/-}$ mice (Figures 7D and 7E). To confirm co-regulation at the time of weaning, we analyzed liver lysates from additional 3- or 4-week-old mice lacking *E2f1, E2f7*, and *E2f8*, or all three genes. Whereas no difference for caspase-2 protein expression could be observed in *E2f1*-deficient tissue samples, levels were strongly increased in *E2f7*$^{-/-}$ and *E2f8*$^{-/-}$ livers. Most importantly, the additional loss of *E2f1* in triple knockout mice reduced caspase-2 expression to WT levels, confirming the proposed autoregulatory feedback loop (Figure 7F).

Taken together, these findings suggest that *CASP2* and *PIDD1* expression is controlled by the counteracting E2F family members E2F1, E2F7 and E2F8. *RAIDD*, however, is not regulated by E2F proteins.

DISCUSSION

Hepatocyte polyploidization is induced at the time of weaning where rapid liver growth meets drastic changes in metabolic load (Celton-Morizur et al., 2009; Pandit et al., 2013). Although the role of hepatocyte ploidy in normal physiology remains uncertain, as changes in either direction do not affect liver size or function, recent evidence suggests tumor suppressive effects. This has been ascribed to increased ploidy slowing down proliferative capacity of hepatocytes (Wilkinson et al., 2018) and generating a reservoir of tumor suppressors (Zhang et al., 2018b, 2018a).

Here, we show that the PIDDosome-p53-p21 axis is activated in hepatocytes where it controls the extent of polyploidization during juvenile development. Timewise, the PIDDosome is activated approximately after the first round of cytokinesis failure in hepatocytes, as indicated by the disappearance of the pro-form of caspase-2, a surrogate marker of its activation (Butt et al., 1998), on day 5 post-weaning (Figure 1). Although not formally demonstrated here, this occurs presumably in response to extra centrosomes (Faggioli et al., 2011). Remarkably, despite the fact that livers from *Casp2*$^{-/-}$ mice contained fewer cells that were on average bigger in size, the overall architecture of the liver parenchyma was unaffected by the noted ploidy increase (Figures 2F–2I). Moreover, serum levels of different enzymes and metabolites reflecting liver function and integrity were not altered significantly in steady-state conditions in young and aged mice lacking the PIDDosome (Figure S1B), again raising the question of the physiological relevance of liver cell ploidy.

As polyploid hepatocytes accumulate extra centrosomes, a hallmark of many cancers, tight cell cycle regulation after failed cytokinesis seems key to secure chromosomal stability in the liver. Proliferation in a polyploid state can increase CIN, either by merotelic kinetochore-microtubule attachments occurring frequently when centrosomes cluster, or multipolar mitoses (Holland and Cleveland, 2009). We analyzed copy number alterations in different polyploid states and found low aneuploidy rates in tetraploid hepatocytes, consistent with findings by Amon and colleagues (Knouse et al., 2014). However, the degree of aneuploidy clearly increased with polyploidy, as shown in octaploid hepatocytes (Figure 3). In hexa-decaploid (16c) hepatocytes we observed an even further increase in copy number alterations, but due to the small relative differences between copy number states, quantitative analysis of these data was of limited statistical robustness (Figures S3A and S3B). Our results clearly demonstrate that aneuploidy increases with the basal ploidy in the liver, yet this only poses a risk for transformation in the presence of an additional oncogenic driver (Zhang et al., 2018a). Although caspase-2 is dispensable for the clearance of aneuploid cells in the healthy liver, its loss indirectly leads to a relative increase in overall aneuploidy owed to higher basal levels of polyploidy. Interestingly, in line with the higher frequency of multipolar mitoses and multinucleated cells, the degree of copy number variations tended to be higher in caspase-2 deficient octaploid hepatocytes after regeneration (Figure 3). Together, this suggests that the PIDDosome limits the risk for hepatocyte transformation. This is consistent with a recent report showing that increased ploidy, here caused by conditional overexpression of Cyclin E1, is sufficient to increase CIN and to drive liver cancer in mice (Aziz et al., 2019).

Similar to development, liver regeneration in the absence of PIDDosome-dependent p53 activation clearly altered the polyploidization dynamics. Despite the different baseline ploidy, the relative increase in polyploidy during liver regeneration was drastically higher in PIDDosome-deficient mice (Figures 1 and 2). We speculate that in addition to impaired p21 induction, this is also a secondary consequence of the higher basal ploidy state in PIDDosome-deficient mice. Highly polyploid mitoses are error prone and lagging chromosomes and chromosomal bridges contribute to an increased rate of cytokinesis failure (Holland and Cleveland, 2009; Lens and Medema, 2019). Consistently, we frequently observed aberrant mitoses and multinucleation in H&E sections of *Casp2*$^{-/-}$ livers, which was barely seen in WT (Figures 3A–3C). While a recent report shows that WT hepatocytes effectively cluster centrosomes *in situ* (Knouse et al., 2018) the up to 2-fold higher ploidy in caspase-2 deficient cells and the corresponding number of extra centrosomes may prime for aberrant mitoses and subsequent defective cell divisions. Hence, the PIDDosome can prevent uncontrolled polyploidization either directly, on demand upon proliferation stress, or as a consequence of its ploidy-limiting action during development.

In the course of liver regeneration, p21 has been reported to be induced by several cues, including DNA damage caused by

(C) *p21* mRNA levels analyzed in hepatocytes also displayed in (A) from indicated genotypes either before (0 h) or 48 h and 7 days after PH.
(D) Representative IHC images (20×) of WT and *Casp2*$^{-/-}$ livers stained for p21 at 48, 72, and 96 h post-PH.
(E) p21 expression was quantified as percentage of low ploid versus polyploid hepatocytes (n = 3). Polyploidy is defined as >2× diameter of pericentral hepatocyte nuclei and binucleated cells. n = 3–6 (Table S7); scale bars represent 100 μm, mean ± SEM; *p < 0.05, **p < 0.01, ***p < 0.001, ****p < 0.0001.

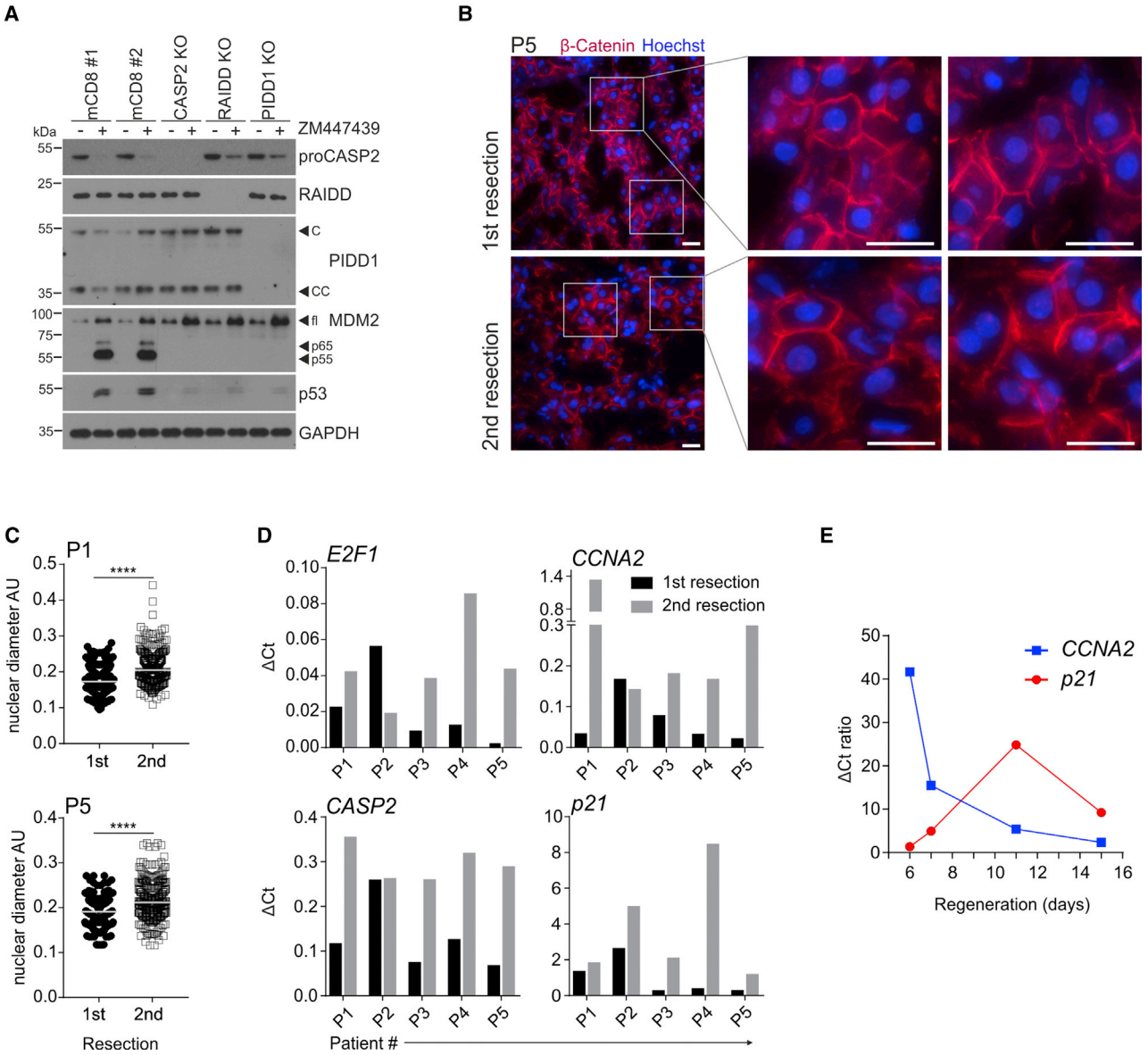

Figure 5. Human Hepatocytes Engage the PIDDosome during Liver Regeneration

(A) HepG2 cells were genome-edited using CRISPR/Cas9 with sgRNAs targeting either mouse CD8 (control) or the individual PIDDosome components. Bulk cultures were treated with ZM447439 or DMSO for 72 h and analyzed by immunoblotting.

(B) Representative images including zoom-ins of cryo-sections from patient #5 undergoing ALPPS, sampled during the first and second resection. The sections were stained for DNA (hoechst 33342) and β-catenin to visualize cell boundaries; scale bar represents 20 μm.

(C) Nuclear size was measured in tissue sections of patients #1 and #5 also shown in (B). Quantification shows increased nuclear size during or after regeneration at the second resection; data are represented as median of all cells measured per patient, ****$p < 0.0001$.

(D) Transcript levels of *E2F1*, *CCNA2*, *CASP2*, and *p21* were assessed in matched RNA samples of ALPPS patients. Tissue biopsies were isolated during the first and second surgery.

(E) *CCNA2* and *p21* levels in patients shown in (D) are displayed based on the time between first and second resection (regeneration time, see Table S1). Due to liver dysfunction and unchanged *CCNA2* levels, indicating no proliferative response during regeneration, patient #2 was excluded from this analysis.

proliferation in a polyploid state (Holland and Cleveland, 2009; Janssen et al., 2011; Karimian et al., 2016). Here, we demonstrate clearly that the at least 3-fold higher p21 levels, predominantly seen in polyploid WT hepatocytes, solely depend on PIDDosome-mediated p53 activation and are likely not a secondary consequence of DNA damage. This results in reduced proliferative capacity of polyploid hepatocytes, a phenomenon that has recently been reported by Wilkinson and colleagues (Wilkinson et al., 2018). We provide evidence that polyploid hepatocytes engage the PIDDosome during the regeneration process to reduce proliferation via p53-mediated p21 induction to avoid excessive polyploidization.

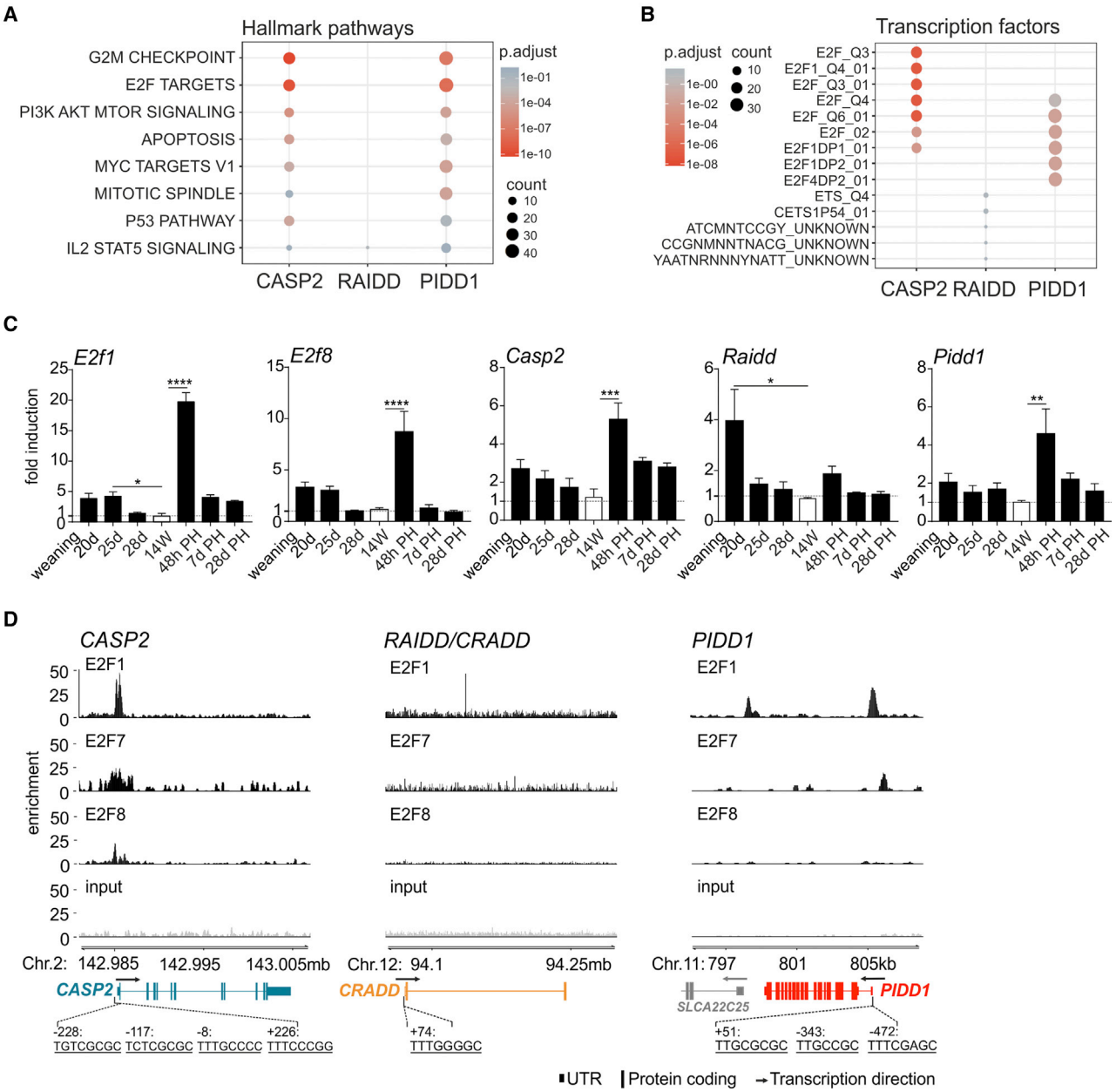

Figure 6. PIDD1 and CASP2 are Co-regulated with E2F Target Genes

(A) STRING data sets were analyzed for genes co-expressed with *CASP2*, *PIDD1*, or *RAIDD*. Co-expressed genes are ordered according to the associated Hallmark pathway (MSigDB) and significance level indicating co-regulation of CASP2 and PIDD1 with E2F targets and other proliferation-related genes.

(B) Co-expressed genes shown in (A) were analyzed for associated transcription factors.

(C) Transcript levels of *E2f1*, *E2f8* and all PIDDosome components in isolated hepatocytes before (20 days) and at indicated time points after weaning, as well as during regeneration. ΔCt values were normalized to the adult, 14-week-old mice (n = 3–7, Table S7).

(D) ChiP-seq analyses for E2F1, E2F7, and E2F8 performed on DNA from HeLa-S3 cells show significant enrichment in the promoter region of *CASP2* and *PIDD1* genes. Data are represented as mean ± SEM; *p < 0.05, **p < 0.01, ***p < 0.001, ****p < 0.0001.

Finally, we demonstrate that *CASP2* and *PIDD1* are dynamically regulated by E2F transcription factors, which directly link PIDDosome activity to hepatocyte proliferation (Figures 6 and 7). The atypical members of this transcription factor family, E2F7 and E2F8 were shown to repress transcription of various genes required for the execution of cytokinesis. The competing E2F1 counteracts the repressors and drives expression of the same target genes. Consistently, liver-specific loss of either E2F1 or E2F7/E2F8 results in hyper- and hypoploidization, respectively (Chen et al., 2012; Pandit et al., 2012). This autoregulatory loop implemented by E2F family members guarantees an ordered polyploidization process by controlling proliferation, on the one hand, and cytokinesis stringency as well as cell-cycle arrest proficiency, on the other. Downregulation of

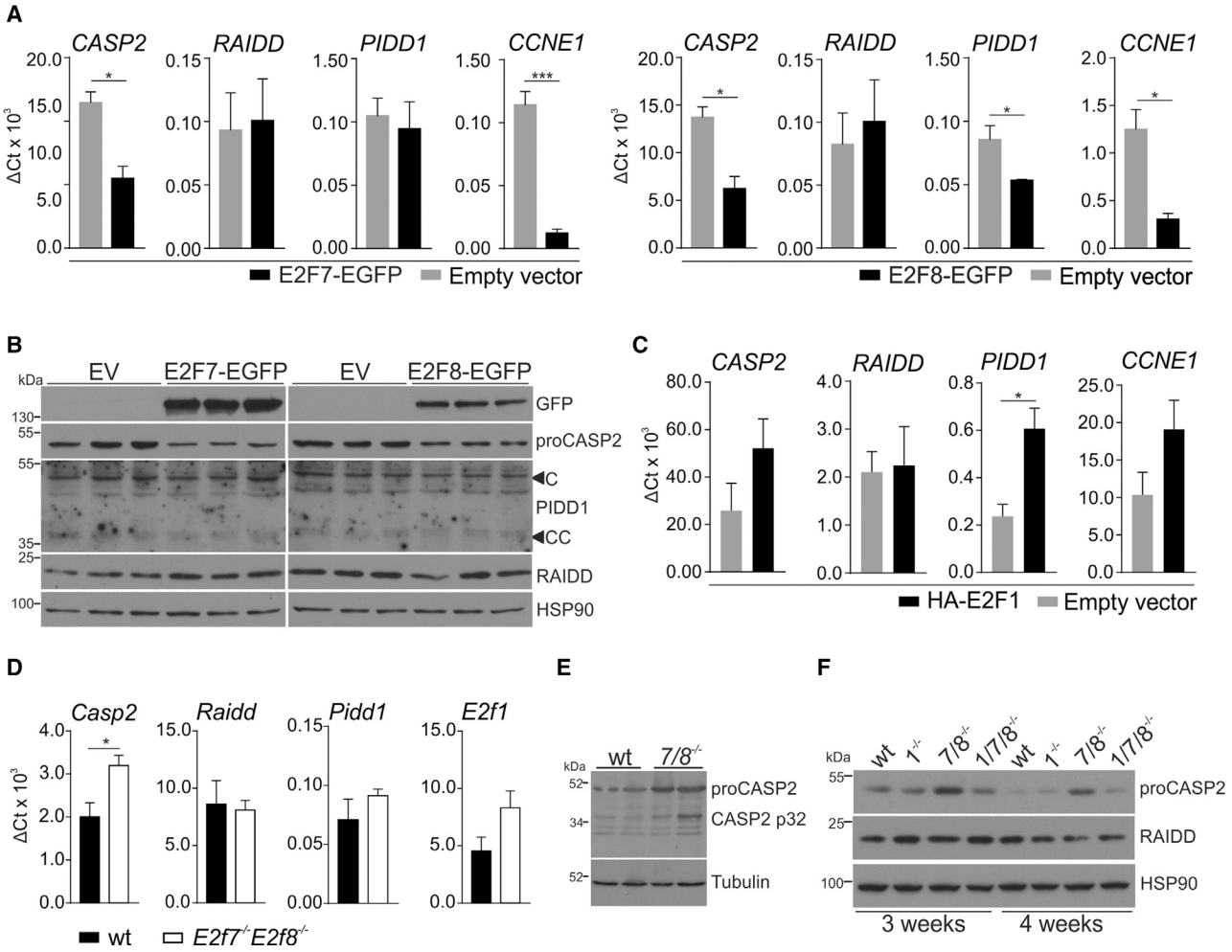

Figure 7. An E2F1/E2F7/E2F8 Autoregulatory Loop Controls PIDD1 and CASP2 Expression Levels

(A) RPE-1 cells carrying constructs allowing doxycycline-inducible expression of E2F7-EGFP, E2F8-EGFP, or empty vector controls, were treated with doxycycline for 24 h, and RNA was isolated and analyzed by qRT-PCR.

(B) Protein lysates from experiments shown in (A) were analyzed by immunoblotting. Quantification of protein levels is shown in Figure S6A.

(C) HepG2 cells were transfected with plasmids encoding HA-E2F1 or an empty vector control for 72 h prior RNA isolation and qRT-PCR analysis. Experiments in (A–C) were performed in three biological replicates and *CCNE1* expression serves as control for E2F function.

(D) Transcript levels of the PIDDosome components in total liver of WT (n = 7) and *E2f7*$^{-/-}$*E2f8*$^{-/-}$ mice (n = 6). *E2F1* levels serve as positive control.

(E) Immunoblots on total liver lysates from 28-day-old mice show increased caspase-2 expression of *E2f7*$^{-/-}$*E2f8*$^{-/-}$ livers (n = 2/genotype).

(F) Immunoblot of total liver lysates of WT and *E2f1*$^{-/-}$, *E2f7*$^{-/-}$*E2f8*$^{-/-}$, *E2f1*$^{-/-}$*E2f7*$^{-/-}$*E2f8*$^{-/-}$ mice at 3 or 4 weeks. Data are represented as mean ± SEM; *p < 0.05, **p < 0.01, ***p < 0.001.

CASP2 by E2F7 and E2F8 is necessary to allow the hepatocytes to reach a physiologically normal, polyploid state. Conversely, re-expression during tissue regeneration, controlled by E2F1, secures an upper limit of ploidy since presence of the PIDDosome in cells carrying extra centrosomes results in its immediate activation. Notably, while two components of the PIDDosome are controlled by E2Fs, the adapter protein RAIDD is regulated differently as the protein remains stable over time, suggesting additional biological roles.

Even though homeostatic proliferation is quite low, hepatocytes need to proliferate to compensate for loss of functional liver parenchyma under pathophysiological conditions, such as fatty liver diseases or viral hepatitis. Compensatory proliferation in these diseases was reported to be accompanied by an increase in polyploidy (Gentric et al., 2015; Toyoda et al., 2005). Interestingly, several reports also show an upregulation of caspase-2 expression levels in human patients as well as in mouse models for non-alcoholic fatty liver disease (NAFLD) and non-alcoholic steatohepatitis (NASH) (Kim et al., 2018; Machado et al., 2015). Aside from its involvement in fat metabolism, these reports confirm that caspase-2 regulation is coupled to proliferation under stress conditions, which have the potential to increase liver ploidy.

Of note, we found that human HCC-derived HepG2 cells also engage the PIDDosome for p53 activation in response to cytokinesis failure. Most importantly, hepatocytes in the regenerating human liver from patients that underwent liver surgery according

to the ALPPS procedure (Schnitzbauer et al., 2012) show a pattern of PIDDosome expression and *p21* induction similar to that observed in mice (Figure 5). This clearly suggests that the same signaling network is employed during human liver regeneration to control hepatocyte polyploidization. Together, these findings strongly suggest that murine and human hepatocytes engage the PIDDosome for ploidy control to avoid adverse effects of excessive polyploidization such as multipolar mitoses and potentially CIN. On the other hand, PIDDosome-mediated p21 induction leads to a delay in liver mass regeneration, which increases the risk of post-surgical complications and infection in humans (Van Den Broek et al., 2008; Rahbari et al., 2011). Of note, it has been shown before that depletion of *p21* suffices to overcome delayed regeneration after extended hepatectomy in mice, a model of the ''small-for-size syndrome'' observed in humans (Lehmann et al., 2012). This finding is especially relevant for patients with a small liver remnant after resection, which might result in liver failure due to impaired or strongly delayed regeneration (small-for-size-syndrome) (Clavien et al., 2010). Hence, reducing p21 levels by inhibition of the PIDDosome could be exploited therapeutically to accelerate liver regeneration.

STAR★METHODS

Detailed methods are provided in the online version of this paper and include the following:

- KEY RESOURCES TABLE
- LEAD CONTACT AND MATERIALS AVAILABILITY
- EXPERIMENTAL MODEL AND SUBJECT DETAILS
  - Human Patient Biopsies
  - Animals
  - Cell Culture
- METHOD DETAILS
  - Partial Hepatectomy
  - Hepatocyte Isolation
  - Immunohistochemistry
  - Histopathological Examination
  - Immunofluorescence
  - Single-Cell Whole Genome Sequencing
  - Single-Cell Sequencing Data Analysis
  - Serum Parameters
  - Cell Lysis and Immunoblotting
  - RNA Isolation and qRT-PCR
  - Ploidy Measurement
  - Generation of Cell Lines
  - Plasmid Transfection
  - ChIP-Seq Data Analysis
  - STRING Data Analysis
- QUANTIFICATION AND STATISTICAL ANALYSIS
  - Statistics and Data Analysis
- DATA AND CODE AVAILABILITY

SUPPLEMENTAL INFORMATION

Supplemental Information can be found online at https://doi.org/10.1016/j.devcel.2019.12.016.

ACKNOWLEDGMENTS

We are grateful to I. Gaggl, K. Rossi, M. Fischer, N. Schöpf, and A. Beierfuß for excellent technical assistance or animal care. We also thank A. Strasser and T. Mak for sharing mouse models and reagents, as well as M. Bergmann, S. Geley, A. Curinha, and G.F. Vogel for fruitful discussions and support with microscopy. This work was supported by the FWF-funded Doctoral College ''Molecular Cell Biology and Oncology'' (W1101) to V.C.S. and F.W.F. Grant nos. P 26856 and PIR 3 and the ERC AdG POLICE (787171) to A.V. L.L.F. acknowledges support by the Giovanni Armenise-Harvard Foundation.

AUTHOR CONTRIBUTIONS

V.C.S. designed and conducted the experiments, wrote the manuscript, and analyzed the data. S.S. assisted with animal experiments. K.K., C.S., J.H., F.E., L.R.R., E.M., and E.A.V.M. performed the experiments. B.W. analyzed the ChiP-seq data. L.B. and A.d.B. performed histological analyses. M.T. enabled hepatectomy experiments. L.F. initiated research and analyzed data. T.G.S. performed bioinformatic analyses. P.S. and D.P. provided ALPPS patient biopsies. B.B., D.S., R.W., and F.F. conducted single-cell whole genome sequencing and analyzed the results. T.S. and H.S. analyzed serum parameters. A.V. designed the research, analyzed the data, wrote the manuscript, and conceived the study.

DECLARATION OF INTERESTS

The authors declare no competing interests.

Received: May 16, 2019
Revised: October 27, 2019
Accepted: December 24, 2019
Published: January 23, 2020

REFERENCES

Abmayr, S.M., and Pavlath, G.K. (2012). Myoblast fusion: lessons from flies and mice. Development *139*, 641–656.

Aziz, K., Limzerwala, J.F., Sturmlechner, I., Hurley, E., Zhang, C., Jeganathan, K.B., Nelson, G., Bronk, S., Fierro Velasco, R.O., van Deursen, E.J., et al. (2019). Ccne1 overexpression causes chromosome instability in liver cells and liver tumor development in mice. Gastroenterology *157*, 210–226.e12.

Bakker, B., Taudt, A., Belderbos, M.E., Porubsky, D., Spierings, D.C.J., de Jong, T.V., Halsema, N., Kazemier, H.G., Hoekstra-Wakker, K., Bradley, A., et al. (2016). Single-cell sequencing reveals karyotype heterogeneity in murine and human malignancies. Genome Biol. *17*, 115.

Berube, C., Boucher, L.M., Ma, W., Wakeham, A., Salmena, L., Hakem, R., Yeh, W.C., Mak, T.W., and Benchimol, S. (2005). Apoptosis caused by p53-induced protein with death domain (PIDD) depends on the death adapter protein RAIDD. Proc. Natl. Acad. Sci. USA *102*, 14314–14320.

Bouchier-Hayes, L., and Green, D.R. (2012). Caspase-2: the orphan caspase. Cell Death Differ. *19*, 51–57.

Brugarolas, J., Chandrasekaran, C., Gordon, J.I., Beach, D., Jacks, T., and Hannon, G.J. (1995). Radiation-induced cell cycle arrest compromised by p21 deficiency. Nature *377*, 552–557.

Butt, A.J., Harvey, N.L., Parasivam, G., and Kumar, S. (1998). Dimerization and autoprocessing of the NEDD2 (caspase-2) precursor requires both the prodomain and the carboxyl-terminal regions. J. Biol. Chem. *273*, 6763–6768.

Cancer Genome Atlas Research Network. (2017). Comprehensive and integrative genomic characterization of hepatocellular carcinoma. Cell *169*, 1327–1341.e23.

Celton-Morizur, S., Merlen, G., Couton, D., Margall-Ducos, G., and Desdouets, C. (2009). The insulin/Akt pathway controls a specific cell division program that leads to generation of binucleated tetraploid liver cells in rodents. J. Clin. Invest. *119*, 1880–1887.

Chen, H.Z., Ouseph, M.M., Li, J., Pécot, T., Chokshi, V., Kent, L., Bae, S., Byrne, M., Duran, C., Comstock, G., et al. (2012). Canonical and atypical E2Fs regulate the mammalian endocycle. Nat. Cell Biol. *14*, 1192–1202.

Chen, H.Z., Tsai, S.Y., and Leone, G. (2009). Emerging roles of E2Fs in cancer: an exit from cell cycle control. Nat. Rev. Cancer *9*, 785–797.

Clavien, P.A., Oberkofler, C.E., Raptis, D.A., Lehmann, K., Rickenbacher, A., and El-Badry, A.M. (2010). What is critical for liver surgery and partial liver transplantation: size or quality? Hepatology *52*, 715–729.

Conner, E.A., Lemmer, E.R., Sánchez, A., Factor, V.M., and Thorgeirsson, S.S. (2003). E2F1 blocks and c-Myc accelerates hepatic ploidy in transgenic mouse models. Biochem. Biophys. Res. Commun. *302*, 114–120.

Dawar, S., Lim, Y., Puccini, J., White, M., Thomas, P., Bouchier-Hayes, L., Green, D.R., Dorstyn, L., and Kumar, S. (2016). Caspase-2-mediated cell death is required for deleting aneuploid cells. Oncogene *36*, 2704–2714.

Denechaud, P.D., Lopez-Mejia, I.C., Giralt, A., Lai, Q., Blanchet, E., Delacuisine, B., Nicolay, B.N., Dyson, N.J., Bonner, C., Pattou, F., et al. (2016). E2F1 mediates sustained lipogenesis and contributes to hepatic steatosis. J. Clin. Invest. *126*, 137–150.

Duncan, A.W., Hanlon Newell, A.E., Bi, W., Finegold, M.J., Olson, S.B., Beaudet, A.L., and Grompe, M. (2012a). Aneuploidy as a mechanism for stress-induced liver adaptation. J. Clin. Invest. *122*, 3307–3315.

Duncan, A.W., Hanlon Newell, A.E., Smith, L., Wilson, E.M., Olson, S.B., Thayer, M.J., Strom, S.C., and Grompe, M. (2012b). Frequent aneuploidy among normal human hepatocytes. Gastroenterology *142*, 25–28.

Duncan, A.W., Taylor, M.H., Hickey, R.D., Hanlon Newell, A.E., Lenzi, M.L., Olson, S.B., Finegold, M.J., and Grompe, M. (2010). The ploidy conveyor of mature hepatocytes as a source of genetic variation. Nature *467*, 707–710.

Durinck, S., Spellman, P.T., Birney, E., and Huber, W. (2009). Mapping identifiers for the integration of genomic datasets with the R/Bioconductor package biomaRt. Nat. Protoc. *4*, 1184–1191.

Faggioli, F., Vezzoni, P., and Montagna, C. (2011). Single-cell analysis of ploidy and centrosomes underscores the peculiarity of normal hepatocytes. PLoS One *6*, e26080.

Fava, L.L., Bock, F.J., Geley, S., and Villunger, A. (2012). Caspase-2 at a glance. J. Cell Sci. *125*, 5911–5915.

Fava, L.L., Schuler, F., Sladky, V., Haschka, M.D., Soratroi, C., Eiterer, L., Demetz, E., Weiss, G., Geley, S., Nigg, E.A., et al. (2017). The PIDDosome activates p53 in response to supernumerary centrosomes. Genes Dev. *31*, 34–45.

Gentric, G., Maillet, V., Paradis, V., Couton, D., L'Hermitte, A.L., Panasyuk, G., Fromenty, B., Celton-Morizur, S., and Desdouets, C. (2015). Oxidative stress promotes pathologic polyploidization in nonalcoholic fatty liver disease. J. Clin. Invest. *125*, 981–992.

Gjelsvik, K.J., Besen-McNally, R., and Losick, V.P. (2019). Solving the polyploid mystery in health and disease. Trends Genet. *35*, 6–14.

Grompe, M., Jones, S.N., Loulseged, H., and Caskey, C.T. (1992). Retroviral-mediated gene transfer of human ornithine transcarbamylase into primary hepatocytes of spf and spf-ash mice. Hum. Gene Ther. *3*, 35–44.

Holland, A.J., and Cleveland, D.W. (2009). Boveri revisited: chromosomal instability, aneuploidy and tumorigenesis. Nat. Rev. Mol. Cell Biol. *10*, 478–487.

Janssen, A., van der Burg, M., Szuhai, K., Kops, G.J.P.L., and Medema, R.H. (2011). Chromosome segregation errors as a cause of DNA damage and structural chromosome aberrations. Science *333*, 1895–1898.

Karimian, A., Ahmadi, Y., and Yousefi, B. (2016). Multiple functions of p21 in cell cycle, apoptosis and transcriptional regulation after DNA damage. DNA Repair (Amst) *42*, 63–71.

Kent, L.N., Rakijas, J.B., Pandit, S.K., Westendorp, B., Chen, H.Z., Huntington, J.T., Tang, X., Bae, S., Srivastava, A., Senapati, S., et al. (2016). E2f8 mediates tumor suppression in postnatal liver development. J. Clin. Invest. *126*, 2955–2969.

Kim, J.Y., Garcia-Carbonell, R., Yamachika, S., Zhao, P., Dhar, D., Loomba, R., Kaufman, R.J., Saltiel, A.R., and Karin, M. (2018). ER stress drives lipogenesis and steatohepatitis via caspase-2 activation of S1P. Cell *175*, 133–145.e15.

Knouse, K.A., Lopez, K.E., Bachofner, M., and Amon, A. (2018). Chromosome segregation fidelity in epithelia requires tissue architecture. Cell *175*, 200–211.e13.

Knouse, K.A., Wu, J., Whittaker, C.A., and Amon, A. (2014). Single cell sequencing reveals low levels of aneuploidy across mammalian tissues. Proc. Natl. Acad. Sci. USA *111*, 13409–13414.

Kumar, S. (2009). Caspase 2 in apoptosis, the DNA damage response and tumour suppression: enigma no more? Nat. Rev. Cancer *9*, 897–903.

Kurinna, S., Stratton, S.A., Coban, Z., Schumacher, J.M., Grompe, M., Duncan, A.W., and Barton, M.C. (2013). P53 regulates a mitotic transcription program and determines ploidy in normal mouse liver. Hepatology *57*, 2004–2013.

Langmead, B., and Salzberg, S.L. (2012). Fast gapped-read alignment with Bowtie 2. Nat. Methods *9*, 357–359.

Lawrence, M., Gentleman, R., and Carey, V. (2009). rtracklayer: an R package for interfacing with genome browsers. Bioinformatics *25*, 1841–1842.

Lawrence, M., Huber, W., Pagès, H., Aboyoun, P., Carlson, M., Gentleman, R., Morgan, M.T., and Carey, V.J. (2013). Software for computing and annotating genomic ranges. PLoS Comput. Biol. *9*, e1003118.

Lehmann, K., Tschuor, C., Rickenbacher, A., Jang, J.H., Oberkofler, C.E., Tschopp, O., Schultze, S.M., Raptis, D.A., Weber, A., Graf, R., et al. (2012). Liver failure After extended hepatectomy in mice is mediated by a p21-dependent barrier to liver regeneration. Gastroenterology *143*, 1609–1619.e4.

Lens, S.M.A., and Medema, R.H. (2019). Cytokinesis defects and cancer. Nat. Rev. Cancer *19*, 32–45.

Li, H., Handsaker, B., Wysoker, A., Fennell, T., Ruan, J., Homer, N., Marth, G., Abecasis, G., and Durbin, R.; 1000 Genome Project Data Processing Subgroup (2009). The Sequence Alignment/Map format and SAMtools. Bioinformatics *25*, 2078–2079.

López-García, C., Sansregret, L., Domingo, E., McGranahan, N., Hobor, S., Birkbak, N.J., Horswell, S., Grönroos, E., Favero, F., Rowan, A.J., et al. (2017). BCL9L dysfunction impairs caspase-2 expression permitting aneuploidy tolerance in colorectal cancer. Cancer Cell *31*, 79–93.

Lowe, S.W., Schmitt, E.M., Smith, S.W., Osborne, B.A., and Jacks, T. (1993). P53 is required for radiation-induced apoptosis in mouse thymocytes. Nature *362*, 847–849.

Machado, M.V., Michelotti, G.A., Pereira, Tde A., Boursier, J., Kruger, L., Swiderska-Syn, M., Karaca, G., Xie, G., Guy, C.D., Bohinc, B., et al. (2015). Reduced lipoapoptosis, hedgehog pathway activation and fibrosis in caspase-2 deficient mice with non-alcoholic steatohepatitis. Gut *64*, 1148–1157.

Manzl, C., Krumschnabel, G., Bock, F., Sohm, B., Labi, V., Baumgartner, F., Logette, E., Tschopp, J., and Villunger, A. (2009). Caspase-2 activation in the absence of PIDDosome formation. J. Cell Biol. *185*, 291–303.

Margall-Ducos, G., Celton-Morizur, S., Couton, D., Brégerie, O., and Desdouets, C. (2007). Liver tetraploidization is controlled by a new process of incomplete cytokinesis. J. Cell Sci. *120*, 3633–3639.

McIlwain, D.R., Berger, T., and Mak, T.W. (2013). Caspase functions in cell death and disease. Cold Spring Harb. Perspect. Biol. *5*, a008656.

Nigg, E.A., and Holland, A.J. (2018). Once and only once: mechanisms of centriole duplication and their deregulation in diseases. Nat. Rev. Mol. Cell Biol. *19*, 297–312.

O'Reilly, L.A., Ekert, P., Harvey, N., Marsden, V., Cullen, L., Vaux, D.L., Hacker, G., Magnusson, C., Pakusch, M., Cecconi, F., et al. (2002). Caspase-2 is not required for thymocyte or neuronal apoptosis even though cleavage of caspase-2 is dependent on both Apaf-1 and caspase-9. Cell Death Differ. *9*, 832–841.

Oliver, T.G., Meylan, E., Chang, G.P., Xue, W., Burke, J.R., Humpton, T.J., Hubbard, D., Bhutkar, A., and Jacks, T. (2011). Caspase-2-mediated cleavage of Mdm2 creates a p53-induced positive feedback loop. Mol. Cell *43*, 57–71.

Otto, S.P. (2007). The evolutionary consequences of polyploidy. Cell *131*, 452–462.

Pandit, S.K., Westendorp, B., and De Bruin, A. (2013). Physiological significance of polyploidization in mammalian cells. Trends Cell Biol. *23*, 556–566.

Pandit, S.K., Westendorp, B., Nantasanti, S., Van Liere, E., Tooten, P.C.J., Cornelissen, P.W.A., Toussaint, M.J.M., Lamers, W.H., and De Bruin, A. (2012). E2F8 is essential for polyploidization in mammalian cells. Nat. Cell Biol. *14*, 1181–1191.

Pang, L., Weiss, M.J., and Poncz, M. (2005). Megakaryocyte biology and related disorders. J. Clin. Invest. *115*, 3332–3338.

Rahbari, N.N., Garden, O.J., Padbury, R., Brooke-Smith, M., Crawford, M., Adam, R., Koch, M., Makuuchi, M., Dematteo, R.P., Christophi, C., et al. (2011). Posthepatectomy liver failure: a definition and grading by the International Study Group of Liver Surgery (ISGLS). Surgery *149*, 713–724.

Sanjana, N.E., Shalem, O., and Zhang, F. (2014). Improved vectors and genome-wide libraries for CRISPR screening. Nat. Methods *11*, 783–784.

Sarkar, D., Gentleman, R., Lawrence, M., and Y.Z. (2018). A package for analyzing chipseq data. R package version 1.32.0.

Schneider, C.A., Rasband, W.S., and Eliceiri, K.W. (2012). NIH Image to ImageJ: 25 years of image analysis. Nat. Methods *9*, 671–675.

Schnitzbauer, A.A., Lang, S.A., Goessmann, H., Nadalin, S., Baumgart, J., Farkas, S.A., Fichtner-Feigl, S., Lorf, T., Goralcyk, A., Hörbelt, R., et al. (2012). Right portal vein ligation combined with in situ splitting induces rapid left lateral liver lobe hypertrophy enabling 2-staged extended right hepatic resection in small-for-size settings. Ann. Surg. *255*, 405–414.

Sheahan, S., Bellamy, C.O., Treanor, L., Harrison, D.J., and Prost, S. (2004). Additive effect of p53, p21 and Rb deletion in triple knockout primary hepatocytes. Oncogene *23*, 1489–1497.

Sigal, S.H., Rajvanshi, P., Gorla, G.R., Sokhi, R.P., Saxena, R., Gebhard, D.R., Reid, L.M., and Gupta, S. (1999). Partial hepatectomy-induced polyploidy attenuates hepatocyte replication and activates cell aging events. Am. J. Physiol. *276*, G1260–G1272.

Sladky, V., Schuler, F., Fava, L.L., and Villunger, A. (2017). The resurrection of the PIDDosome – emerging roles in the DNA-damage response and centrosome surveillance. J. Cell Sci. *130*, 3779–3787.

Subramanian, A., Tamayo, P., Mootha, V.K., Mukherjee, S., Ebert, B.L., Gillette, M.A., Paulovich, A., Pomeroy, S.L., Golub, T.R., Lander, E.S., et al. (2005). Gene set enrichment analysis: a knowledge-based approach for interpreting genome-wide expression profiles. Proc. Natl. Acad. Sci. USA *102*, 15545–15550.

Szklarczyk, D., Gable, A.L., Lyon, D., Junge, A., Wyder, S., Huerta-Cepas, J., Simonovic, M., Doncheva, N.T., Morris, J.H., Bork, P., et al. (2019). STRING v11: protein–protein association networks with increased coverage, supporting functional discovery in genome-wide experimental datasets. Nucleic Acids Res. *47*, D607–D613.

Tachibana, K.E., Gonzalez, M.A., Guarguaglini, G., Nigg, E.A., and Laskey, R.A. (2005). Depletion of licensing inhibitor geminin causes centrosome overduplication and mitotic defects. EMBO Rep. *6*, 1052–1057.

Tang, Y.C., and Amon, A. (2013). Gene copy-number alterations: a cost-benefit analysis. Cell *152*, 394–405.

Tinel, A., and Tschopp, J. (2004). The PIDDosome, a protein complex implicated in activation of caspase-2 in response to genotoxic stress. Science *304*, 843–846.

Toyoda, H., Bregerie, O., Vallet, A., Nalpas, B., Pivert, G., Brechot, C., and Desdouets, C. (2005). Changes to hepatocyte ploidy and binuclearity profiles during human chronic viral hepatitis. Gut *54*, 297–302.

van den Bos, H., Bakker, B., Taudt, A., Guryev, V., Colomé-Tatché, M., Lansdorp, P.M., Foijer, F., and Spierings, D.C.J. (2019). Quantification of aneuploidy in mammalian systems. Methods Mol. Biol. *1896*, 159–190.

Van Den Broek, M.A.J., Olde Damink, S.W.M., Dejong, C.H.C., Lang, H., Malagó, M., Jalan, R., and Saner, F.H. (2008). Liver failure after partial hepatic resection: definition, pathophysiology, risk factors and treatment. Liver Int. *28*, 767–780.

Wang, J., Batourina, E., Schneider, K., Souza, S., Swayne, T., Liu, C., George, C.D., Tate, T., Dan, H., Wiessner, G., et al. (2018). Polyploid superficial cells that maintain the urothelial barrier are produced via incomplete cytokinesis and endoreplication. Cell Rep. *25*, 464–477.e4.

Wickham, H. (2009). ggplot2 (Springer).

Wilkinson, P.D., Delgado, E.R., Alencastro, F., Leek, M.P., Roy, N., Weirich, M.P., Stahl, E.C., Otero, P.A., Chen, M.I., Brown, W.K., et al. (2018). The polyploid state restricts hepatocyte proliferation and liver regeneration. Hepatology *69*, 1242–1258.

Yu, G., Wang, L.G., Han, Y., and He, Q.Y. (2012). clusterProfiler: an R package for comparing biological themes among gene clusters. OMICS A J. Integr. Biol. *16*, 284–287.

Zhang, S., Nguyen, L.H., Zhou, K., Tu, H.C., Sehgal, A., Nassour, I., Li, L., Gopal, P., Goodman, J., Singal, A.G., et al. (2018b). Knockdown of Anillin actin binding protein blocks cytokinesis in hepatocytes and reduces liver tumor development in mice without affecting regeneration. Gastroenterology *154*, 1421–1434.

Zhang, S., Zhou, K., Luo, X., Li, L., Tu, H.C., Sehgal, A., Nguyen, L.H., Zhang, Y., Gopal, P., Tarlow, B.D., et al. (2018a). The polyploid state plays a tumor-suppressive role in the liver. Dev. Cell *44*, 447–459.e5.

Zhang, Y., Liu, T., Meyer, C.A., Eeckhoute, J., Johnson, D.S., Bernstein, B.E., Nusbaum, C., Myers, R.M., Brown, M., Li, W., et al. (2008). Model-based analysis of ChIP-Seq (MACS). Genome Biol. *9*, R137.

Zhu, L.J., Gazin, C., Lawson, N.D., Pagès, H., Lin, S.M., Lapointe, D.S., and Green, M.R. (2010). ChIPpeakAnno: a bioconductor package to annotate ChIP-seq and ChIP-chip data. BMC Bioinformatics *11*, 237.

STAR★METHODS

KEY RESOURCES TABLE

REAGENT or RESOURCE	SOURCE	IDENTIFIER
Antibodies		
Rat monoclonal anti Casp2 (11B4)	Enzo Life Science	Cat# ALX-804-356; RRID:AB_2275199
Mouse monoclonal anti PIDD1 (Anto-1)	Enzo Life Science	Cat# ALX-804-837; RRID:AB_2297204
Rabbit polyclonal anti-RAIDD	Proteintech	Cat# 10401-1-AP; RRID:AB_2085477
Rabbit polyclonal anti p21 (M-19)	Santa Cruz Technologies	Cat# sc-471; RRID:AB_632123
Mouse monoclonal anti p53 (1C12)	Cell Signaling Technology	Cat# 2524; RRID:AB_331743
Mouse monoclonal anti E2F-1 (KH95)	Santa Cruz Technologies	Cat# sc-251; RRID:AB_627476
Mouse monoclonal anti-CyclinB1 (V152)	Abcam	Cat# ab72,; RRID:AB_305751
Mouse monoclonal anti MDM2 (IF2)	Thermo Fisher Scientific	Cat# 33-7100; RRID:AB_2533136
Mouse monoclonal anti Hsp90	Santa Cruz Technologies	Cat# sc-13119; RRID:AB_675659
Rabbit monoclonal anti GAPDH (14C10)	Cell Signaling Technology	Cat# 2118; RRID:AB_561053
Rabbit monoclonal anti cleaved caspase-3 (5A1E)	Cell Signaling Technology	Cat# 9661S; RRID:AB_2341188
HRP-mouse anti rat	Cell Signaling Technology	Cat# 7077; RRID:AB_10694715
HRP-rabbit anti mouse	Agilent	Cat# P0161; RRID:AB_2687969
HRP-goat anti rabbit	Agilent	Cat# P0448; RRID:AB_2617138
Biotin-goat anti rabbit	Vector laboratories	Cat# BA-1000; RRID:AB_2313606
Mouse monoclonal anti ßcatenin (14)	BD Bioscience	Cat# 610154; RRID:AB_397555
Alexa flour 546 goat anti mouse	Thermo Fisher	Cat# A-11030; RRID:AB_2534089
Bacterial and Virus Strains		
DH5 alpha	Lab of Stephan Geley	N/A
XL1-Blue MR Supercompetent Cells	Agilent	2002229
Biological Samples		
Human liver biopsies (ALPPS)	Patrick Starlinger, Medical University of Vienna, A	N/A
Liver tissue samples from FVB wt, FVB *E2f1*$^{-/-}$, FVB *E2f7*$^{-/-}$*E2f8*$^{-/-}$, FVB *E2f1*$^{-/-}$*E2f7*$^{-/-}$*E2f8*$^{-/-}$ mice	Lab of Alain de Bruin, Utrecht University, NL	N/A
Chemicals, Peptides, and Recombinant Proteins		
Isoflurane (Forane ®)	AbbVie	CAS# 26675-46-7
Buprenorphine (Temgesic)	Indivior UK Limited	CAS# 52485-79-7
Ketamine	AniMedica	CAS# 1867-66-9
Xylazine	AniMedica	CAS# 0007361-61-7
Piritramid (Dipidolor)	Piramal Critical Care	CAS# 302-41-0
Liberase TM	Sigma-Aldrich	#5401119001
DMEM	Sigma-Aldrich	D5671
FBS (fetal bovine serum)	PAA laboratories	A15-151
L-glutamine	PAA laboratories	M11-00
Penicillin/Streptomycin	PAA laboratories	P11-010
TissueTek O.C.T.	Sakura Europe	#4583
Hoechst 33342	Sigma-Aldrich	CAS#: 23491-52-3
ZM447439	Selleck Chemicals	S1103
PEI (Polyethylenimine)	Sigma-Aldrich	CAS#: 9002-98-6
Puromycin	Sigma-Aldrich	P8833
Blasticidine	Sigma-Aldrich	P15205
Phusion polymerase	New England Biolabs	M0530
BamHI	New England Biolabs	R3136S

(*Continued on next page*)

Continued

REAGENT or RESOURCE	SOURCE	IDENTIFIER
XbaI	New England Biolabs	R0145S
Doxycycline	Sigma-Aldrich	CAS#: 24390-14-5
Oligofectamine	Life Technologies	12252-011
Optimem	Life Technologies	31985-054
Metafectene	Biontex	T020-0.2
EDTA free protease inhibitor cocktail	Roche	11836170001
DNaseI	Sigma-Aldrich	4716728001
Bradford reagent	Bio-rad	500-0006
TRIzol reagent	Ambion, LifeTechnologies	15596018
AceQ qPCR SYBR Green Master Mix	Vazyme	Q131-02
AceQ qPCR Probe Master Mix	Vazyme	Q112-02
Critical Commercial Assays		
Vectastain ABC Kit	Vector Laboratories	PK-6100
ImmPACT DAB	Vector Laboratories	SK-4105
Gibson Assembly® Cloning Kit	New England Biolabs	E5510S
Plasmid Midi Kit	Qiagen	12143
iScript cDNA synthesis kit	Bio-rad	170-8891
Deposited Data		
Single cell whole genome sequencing data	This paper	PRJEB3254 https://www.ebi.ac.uk/ena
Single cell whole genome sequencing profile plots	This paper; Mendeley data	[https://doi.org/10.17632/vfpgvhcvh5.1]
ChiP-seq E2F1, HeLaS3	The ENCODE project	ENCSR000EVJ https://www.encodeproject.org/
ChiP-seq E2F7 and E2F8, HeLaS3	Pandit et al., 2012	GSE32673 https://www.ncbi.nlm.nih.gov/geo/
ChiP-seq E2F1 primary mouse hepatocytes	Denechaud et al., 2016	GSE74006 https://www.ncbi.nlm.nih.gov/geo/
Experimental Models: Cell Lines		
HEK293T (female)	Lab of Alain de Bruin	RRID: CVCL_0063
HepG2 (male)	Lab of Lukas Huber	RRID: CVCL_0027
RPE-hTert (female)	Lab of Alain de Bruin	RRID: CVCL_4388
Experimental Models: Organisms/Strains		
C57BL/6N Casp2$^{-/-}$	O'Reilly et al., 2002	N/A
C57BL/6N Pidd1$^{-/-}$	Manzl et al., 2009	N/A
C57BL/6N Raidd$^{-/-}$	Berube et al., 2005	N/A
C57BL/6N p53$^{-/-}$	Lowe et al., 1993	N/A
C57BL/6N p21$^{-/-}$	Brugarolas et al., 1995	N/A
Oligonucleotides		
mCasp2 fw: TCTCACATGGTGTGGAAGGT	This paper	N/A
mCasp2 fw: AGGGGATTGTGTGTGGTTCT	This paper	N/A
m p21 fw: AATTGGAGTCAGGCGCAGAT	This paper	N/A
m p21 rev: CATGAGCGCATCGCAATCAC	This paper	N/A
PIDD1 predesigned qPCR probe assay	Integrated DNA Technologies	Hs.PT.58.3199598.gs
GAPDH predesigned qPCR probe assay	Integrated DNA Technologies	Hs.PT.39a.22214836
Additional oligonucleotides are reported in Table S2		
Recombinant DNA		
LentiCRISPRv2	Feng Zhang lab	Addgene Plasmid #52961
pMDLg pRRE	Didier Trono	Addgene plasmid #12251

(*Continued on next page*)

Continued

REAGENT or RESOURCE	SOURCE	IDENTIFIER
pCMV-VSV-G	Bob Weinberg	Addgene plasmid #8454
pRSV Rev	Didier Trono	Addgene plasmid #12253
pLenti CMV TetR (716-1)	Eric Campeau & Paul Kaufman	Addgene Plasmid #17492
pLenti CMV/TO Puro DEST (670-1)	Eric Campeau & Paul Kaufman	Addgene Plasmid # 17293
pCDNA3.1-HA-E2F1	Bart Westendorp	N/A
pCDNA3.1-HA	Sebastian Herzog	N/A
Software and Algorithms		
ImageJ	Schneider et al., 2012	https://imagej.nih.gov/ij/
Prism 7.00	Graphpad software	https://www.graphpad.com/
Cell^B (v2.7)	Olympus soft imaging solutions	https://www.olympus-sis.com
VisiView 4.1.0.3	Visitron Systems	https://www.visitron.de
FlowJo X	LLC	https://www.flowjo.com/solutions/flowjo/
R (v3.6.1)	RCore Team	https://www.r-project.org/
ChIPpeakAnno	Zhu et al., 2010	https://bioconductor.org/packages/release/bioc/html/ChIPpeakAnno.html
GenomicRanges	Lawrence et al., 2013	https://bioconductor.org/packages/release/bioc/html/GenomicRanges.html
IRanges	Lawrence et al., 2009	https://bioconductor.org/packages/release/bioc/html/IRanges.html
biomaRt	Durinck et al., 2009	https://bioconductor.org/packages/release/bioc/html/biomaRt.html
Chipseq	Sarkar et al., 2018	https://bioconductor.org/packages/release/bioc/html/chipseq.html
Rtracklayer	Lawrence et al., 2009	https://bioconductor.org/packages/release/bioc/html/rtracklayer.html
SAMtools (v0.1.18)	Li et al., 2009	http://www.htslib.org
Bowtie2 (v2.3.4.3)	Langmead and Salzberg, 2012	https://sourceforge.net/projects/bowtie-bio/files/bowtie2/
AneuFinder (developer version 1.10.1)	Bakker et al., 2016	https://bioconductor.org/packages/release/bioc/html/
clusterProfiler_3.12.0	Yu et al., 2012	https://bioconductor.org/packages/clusterProfiler/
MSigDB (v7.0)	Subramanian et al., 2005	http://software.broadinstitute.org/gsea/msigdb
ggplot2 v3.2.0	Wickham, 2009	http://ggplot2.org

LEAD CONTACT AND MATERIALS AVAILABILITY

Further information and requests for reagents should be directed to and will be fulfilled by the Lead Contact, Dr. Andreas Villunger (andreas.villunger@i-med.ac.at).

EXPERIMENTAL MODEL AND SUBJECT DETAILS

Human Patient Biopsies

Biopsy sampling was approved by the Institutional Ethics Committee at the Medical University of Vienna (#2032/2013) and all patients gave written informed consent. All patients underwent ALPPS procedure (associating liver partition and portal vein ligation for staged hepatectomy). Briefly, ligation of the portal venous branch for the right liver lobe combined with parenchymal transection in a first step lead to augmented liver regeneration. In a second step, approximately 5–15 days after the first step, the previously ligated liver lobe was resected (Schnitzbauer et al., 2012). Biopsies were sampled from the regenerating lobe at the beginning of each the first and second surgery. Five patients diagnosed with metastatic colorectal carcinoma were analyzed for mRNA levels. Cryo-sections derived from patients #1 and #5 were used for ploidy analysis. Details and clinical characteristics of these patients are provided in Table S1.

Animals

All animal experiments were approved by the Austrian Bundesministerium für Bildung, Wissenschaft und Forschung (Tierversuchsgesetz, 2012, BGBl I Nr. 114/2012, GZ 66.011/0093/-WF/V/3b/2016). Generation and genotyping of Casp2$^{-/-}$, Pidd1$^{-/-}$, Raidd$^{-/-}$, p53$^{-/-}$ and p21$^{-/-}$ mice were described before (Berube et al., 2005; Brugarolas et al., 1995; Lowe et al., 1993; Manzl et al., 2009; O'Reilly et al., 2002). The mice used were backcrossed and maintained on a C57BL/6N background for at least 12 generations and housed at the Medical University of Innsbruck. Only male mice were used for partial hepatectomy. Mice used for ploidy analysis before and after weaning as well as aged animals were sex balanced and analyzed at indicated time points. *E2f1*$^{-/-}$, *E2f7*$^{-/-}$*E2f8*$^{-/-}$, *E2f1*$^{-/-}$*E2f7*$^{-/-}$*E2f8*$^{-/-}$ and the corresponding wt mice were kept on an FVB background as described before (Pandit et al., 2012). Liver tissue samples from these mice were collected in Alain de Bruin's lab at Utrecht University, approved by the Utrecht University Animal Ethics Committee and in accordance with institutional and national guidelines. For details on age of the mice used refer to the respective figure legends or Table S7.

Cell Culture

HEK293T (RRID: CVCL_0063; female), HepG2 (RRID: CVCL_0027; male) and hTert-RPE-1 (RRID: CVCL_4388; female) cell lines were cultured at 37 °C with 5% CO2 in DMEM (Sigma-Aldrich, D5671) supplemented with 10% fetal bovine serum (FBS, PAA Laboratories, A15-151), 1% L-glutamine (PAA Laboratories, M11-004), 100 U/ml penicillin and 100 μg/ml streptomycin (PAA Laboratories, P11-010). Cytokinesis failure was induced by treatment with 1 μM ZM447439 (Selleck Chemicals, S1103) 24 h after seeding. Cells were harvested by trypsinization. All cell culture experiments were performed in three independent biological replicates.

METHOD DETAILS

Partial Hepatectomy

68% partial hepatectomy was performed according to Lehmann et al. (Lehmann et al., 2012). Mice were weighted and anesthetized by isoflurane inhalation (2-4%). For analgesia, burprenorphine (0.1 mg/kg BW) was injected s.c. 30 min before surgery. The mouse was incised at the *linea alba*. Following liver ligament removal, cholecystectomy was performed (Prolene, 9⁄0; Ethicon, Neuchatel, Switzerland). Subsequently, the lateral left, middle left and middle right lobe was individually ligated (silk, 6/0) and resected. During the procedure, anesthesia was monitored by reflexes, respiratory rate, and depth as well as color of mucous membranes and inner organs. Mice were allowed to recover on a heating pad and caged individually. After surgery, drinking water was supplemented with piritramid (0.06 mg/ml) and buprenorphine was injected s.c. up to 72h.

Hepatocyte Isolation

Primary mouse hepatocytes were isolated using a two-step collagenase perfusion adapted from (Grompe et al., 1992). In brief, mice were anaesthetized (Ketamine/Xylasole i.p.), the *vena cava inferior* was canulated, clamped below the heart and the portal vein was incised. The liver was perfused with 70 ml (37 °C) perfusion buffer (0.14 M NaCl, 6.7 mM KCl, 10 mM Hepes, 0.1 mM EGTA, pH=7.4) at 7 ml/min and 40 ml collagenase buffer (66.7 mM NaCl, 6.7 mM KCl, 4.7 mM $CaCl_2$*$2H_2O$, 10 mM Hepes, pH=7.45) containing 25 μg/ml Liberase TM (Roche), 37 °C at 2.5 ml/min. The liver was gently disrupted in ice cold DMEM (Sigma-Aldrich, D5671) supplemented with 10 % FCS and 2 mM L-glutamine and the cell suspension was passed through a 100-μm cell strainer. Hepatocytes were separated from non-viable and non-parenchymal cells by three subsequent low speed centrifugations (30 g, 3 min) in the above described medium. Purity and yield of the isolation were assessed by light microscopy. Subsequently, cells were fixed in 70 % ethanol prior to ploidy measurement.

Immunohistochemistry

For immunostaining, tissue sections were deparaffinized and rehydrated in xylol and ethanol. Antigen retrieval was performed using 10-mM citrate buffer (pH 6.0). Following a blocking step in peroxidase solution (1% H_2O_2/TBS), sections were stained consecutively with primary and secondary antibody diluted in 5% goat serum/TBS. VECTASTAIN ABC Kit (Vector Laboratories, Cat# PK-6100) and ImmPACT DAB (Vector Laboratories, Cat# SK-4105) were used for amplification and development, respectively. After counterstaining with hematoxylin and dehydration, sections were mounted and images acquired on an Olympus BX45 microscope using cell^B software (version 2.7, Olympus Soft Imaging Solutions). All images were blinded before analysis.

Histopathological Examination

Histological analyses were performed by a board-certified veterinary pathologist. H&E stained 4-μm sections of paraffin-embedded liver were examined. Polyploidy was histologically defined as >2 times the nuclear diameter of pericentral hepatocytes as well as by counting binucleated cells. Mitotic index was determined by count of mitoses in 10 randomly selected fields (40x). The number of cells positive for active caspase-3 or p21-positive hepatocytes was assessed manually in 5 randomly chosen fields at 20× magnification. The total number of cells and positively stained cells, total number and p21-positive binucleated or cells with larger nuclei were measured using manually drawn masks (ImageJ, Schneider et al., 2012) and counted. Binucleated cells and hepatocytes with nuclei of at least twice the diameter as small, pericentral hepatocyte nuclei were considered as polyploid (Figure 2). Hepatocytes below this threshold were classified as low ploid. Images were acquired on an Olympus BX45 microscope using cell^B software (version 2.7, Olympus Soft Imaging Solutions). All images were blinded before analysis.

Immunofluorescence

Cryo-sections of TissueTek O.C.T. (Sakura Europe) embedded human liver biopsies were fixed in 4 % paraformaldehyde/PBS, stained for β-catenin (Alexa Fluor 546) and DNA (hoechst 33342) and mounted in Mowiol. Images were acquired on a Zeiss Axiovert 200M microscope with an oil immersion objective (PL APO 63× 1.4 oil, Zeiss). The acquisition software VisiView 4.1.0.3 (Visitron Systems) was also used to generate maximum intensity projections of Z-stacks. Contrast and brightness of the images were adjusted with ImageJ (Schneider et al., 2012). The same software was used to determine nuclear size by manually drawn masks in a blinded fashion.

Single-Cell Whole Genome Sequencing

Snap-frozen liver tissue or suspension of isolated hepatocytes were used to isolate nuclei for sorting and sequencing as described by van den Bos et al. (2019). Hepatocyte suspensions were stored in FBS with 10% DMSO at -80 °C until further processing. Cells were thawed and immediately treated with nuclei staining buffer for cell lysis (100 mM Tris-HCl pH7.4, 154 mM NaCl, 1 mM CaCl2, 0.5 mM MgCl2, 0.2% bovine serum albumin, 0.1% NP40 in UltraPure water, 10 μg/ml hoechst 33358 and 10 μg/ml propidium iodide). Alternatively, snap frozen liver tissues were cut with a scalpel into small tissue pieces and incubated in nuclei isolation buffer (10 mM Tris-HCl pH8.0, 320 mM sucrose, 5 mM CaCl2, 3 mM Mg(Ac)2, 0.1 mM EDTA, 1 mM DTT, 0.1% Triton X-100). Nuclei were subsequently gently pushed out of the tissue pieces through a 70 μm filter using a syringe plunger. After centrifugation, nuclei were re-suspended into PBS containing 2% bovine serum albumin and 10 μg/ml hoechst 33358 and 10 μg/ml propidium iodide. Sorting of single nuclei and library preparation were conducted as described previously (Bakker et al., 2016; van den Bos et al., 2019). Sequencing was performed using a NextSeq 500 (Illumina).

Single-Cell Sequencing Data Analysis

Single-cell whole genome sequencing and data were aligned to the murine reference genome (GRCm38) using Bowtie2 (v2.2.4) (Langmead and Salzberg, 2012; Li et al., 2009). For data analysis the developer version of AneuFinder 1.10.1 was used (Bakker et al., 2016). Following GC-correction, blacklisting of artifact-prone regions (extreme low or high coverage in control samples) and mappability checks, libraries were analyzed using the edivisive copy number calling algorithm using the following settings: fixed ground ploidy adjusted for ploidy state of the respective sample, variable bins (average size of 2Mb), 500kb step size, significance level of 0.05 and R equal to 20 (default). Breakpoints that were located within 5 Mb from each other (across libraries) were grouped and centered using custom made R functions. To exclude low quality libraries an additional data curation step was introduced based on total read counts and spikiness of the data, which reflect data variance. Low quality libraries are expected to have a relatively high number of segments and therefore also a high value for spikiness (one of the quality features of AneuFinder). Libraries above a spikiness of >0.11 or total read counts <0.25 Mb were excluded (Figure S3B).

The degree of aneuploidy for each library was calculated as the weighted average of the absolute difference between the observed and expected copy number of each bin. The expected copy number is equal to the copy number of the euploid genome. The aneuploidy score of the sample is the average of all the libraries of the same sample.

Serum Parameters

Serum levels of aspartate aminotransferase (AST), alanine aminotransferase (ALT), total bilirubin, urea, cholesterol and triglycerides were measured enzymatically (Roche Diagnostics, Mannheim, Germany) on a cobas analyzer from Roche.

Cell Lysis and Immunoblotting

All samples were lysed in lysis buffer containing 50 mM Tris pH 8.0, 150 mM NaCl, 0.5% NP-40, 50 mM NaF, 1 mM Na3VO4, 1 mM PMSF, 1 tablet protease inhibitors (EDTA free, Roche) per 10 ml and 30 μg/ml DNaseI (Sigma-Aldrich). Protein concentration was determined using Bradford reagent (Bio-Rad, 500-0006). 50–100 μg of total protein was used for western blotting (AmershamTM HybondTM - ECL nitrocellulose membranes, GE Healthcare) using a wet-transfer system (BioRad). Immunoblots in Figure 7B were quantified using ImageJ.

RNA Isolation and qRT-PCR

Total RNA extraction was performed using Trizol reagent (Ambion, LifeTechnologies, 15596018) according to the manufacturer. 500 ng total RNA was used for generation of cDNA (iScript cDNA synthesis kit, BioRad, 170–8891). Quantitative real-time PCR was performed using either Vazyme, AceQ qPCR SYBR Green Master Mix (Q131-02) or Vazyme, AceQ qPCR Probe Master Mix (Q112-02) on a StepOne Plus real time PCR system (Applied Biosystems). Human PIDD1 was determined using a predesigned probe assay (PIDD1: Hs.PT.58.3199598.gs; GAPDH Hs.PT.39a.22214836; Integrated DNA Technologies). Relative expression was calculated relative to a reference gene using the ΔΔCt method. GAPDH and HPRT served as reference genes for mouse and human samples, respectively.

Ploidy Measurement

Cell suspensions were fixed with 70 % ethanol in PBS at -20°C for at least 30 min. Fixed cells were washed twice with PBS, filtered over a 100-μm cell strainer and stained with 40 μg/ml propidium iodide for 15 min or longer at 37 °C in the presence RNase A. The DNA content was measured on a flow cytometer (LSR-Fortessa, BD Biosystems) and data were analyzed quantitatively, excluding doublets, using FlowJo (FlowJo X, LLC).

Generation of Cell Lines

The CRISPR/Cas9 mediated knock out of *CASP2*, *PIDD1* and *RAIDD* was performed using LentiCRISPRv2 backbone for vector production (gift from Feng Zhang; Addgene plasmid number 52961) (Sanjana et al., 2014). The small guide RNAs targeting the genes of interest were designed using CRISPR Design (http://crispr.mit.edu) and described before (Fava et al., 2017). Cloning was done as described in the protocol from Feng Zhang available at http://www.addgene.org. For transformation DH5alpha bacteria were used. Lentiviral supernatants were produced in 293T packaging cells. After sequence-verification, cells were transfected with the plasmids generated before, together with the packaging plasmids pCMV-VSV-G and psPAX2 using 1 mg/ml polyethylenimine (PEI) at a ratio 1:2 DNA:PEI. The human hepatoma cells (HepG2) were incubated with the lentiviral supernatants and selected with 1 μg/ml puromycin for one week. Polyclonal (bulk) lines were characterized for depletion of target genes by immunoblotting and directly used in the experiments.

Mouse E2F7-EGFP and E2F8-EGFP and EGFP cDNA was amplified (Phusion polymerase; New England Biolabs) and cloned into the pLenti CMV/TO plasmid using the Gibson Assembly® Cloning Kit (New England Biolabs E5510S) according to the manufacturer's instructions. For plasmid amplification, XL1-Blue MR Supercompetent Cells (Agilent) were transformed. Subsequently, plasmids were purified (Qiagen), control-digested (BamHI and XbaI) and the correct sequence was verified by sequencing (Macrogen). Generation of inducible cell lines was performed by introducing consecutively the pLenti CMV TetR and the respective E2F-containing plasmids into retinal pigment epithelium cells (RPE-hTert) cells using a third generation lentiviral packaging system. pLenti CMV TetR Blast (716–1) and pLenti CMV/TO Puro DEST (670–1) were a gift from Eric Campeau & Paul Kaufman to Alain de Bruin's lab (Addgene plasmids #17492; http://n2t.net/addgene:17492; RRID:Addgene_17492; and # 17293 ; http://n2t.net/addgene:17293 ; RRID:Addgene_17293). HEK293T were transfected with 10μg packaging plasmids at 70% confluency. pMDLg pRRE, pCMV-VSV-G, pRSV Rev, were mixed in a ratio 1:1:1 and transfected together with the pLenti constructs using polyethylenimine (PEI). Virus containing supernatant was used for infection of preseeded RPE-hTert cells with addition of 4 μg/mL polybrene. The medium was replaced by fresh DMEM containing 1% Pen-Strep and 10% Tet System Approved FBS after 16h. 20 μg/mL Blasticidine and 20 μg/mL Puromycine were used to select for cells which stably integrated the constructs. Monoclonal colonies were expanded and analyzed for high expression of the Tet-Repressor. Finally, the single-cell derived colonies with highest Tet-Repressor expression were infected with E2F7/8-EGFP. To ensure high Tet-Repressor expression (RPE-TetR), single-cell derived colonies were picked and analyzed by qPCR and screened for Tet-Repressor expression before proceeding to infection with E2F7/8-EGFP and EGFP constructs. To induce overexpression, cells were treated with 0.2μg/mL doxycycline (Sigma Aldrich) for 24h.

Plasmid Transfection

3 x10^6 HepG2 cells per 6 cm dish were transfected with 6 μg plasmid DNA (pCDNA3.1-HA-E2F1 or pCDNA3.1-HA) using Metafectene (Biontex) following the manufacturer's instructions 2.5 h after seeding. Cells were harvested and processed 72 h later.

ChIP-Seq Data Analysis

ChIP-sequencing peaks were called using MACS version 1.4.2 (Zhang et al., 2008) with a p value cutoff of 1E-5. Fold enrichments were calculated over their respective input controls. For E2F1, we used data generated in HeLa-S3 (ENCSR000EVJ) from the ENCODE project. Data for primary mouse hepatocytes transfected with human HA-E2F1 were retrieved from the NCBI's Gene Expression Omnibus (GEO) database under the accession numbers GSE74006. For E2F7 and -8 in HeLa-S3, we used the dataset previously published by Alain de Bruin's lab (GSE32673). The peaks within 1 kb upstream or downstream of transcription start sites were annotated to the human genome (Hg19) using the R package ChIPpeakAnno (Zhu et al., 2010). Figures were created using the Bioconductor packages ''GenomicRanges'', ''IRanges'', ''rtracklayer'', ''bioaRt'', and ''chipseq'' (Durinck et al., 2009; Lawrence et al., 2009, 2013; Sarkar et al., 2018)

STRING Data Analysis

Genes co-expressed with *CASP2*, *RAIDD* and *PIDD1* were downloaded from the STRING database (https://string-db.org/) and filtered for a confidence score of co-expression greater than 0.05 (Szklarczyk et al., 2019). Most relevant terms related to the resulting gene lists were identified with the ''enricher'' function of clusterProfiler in R (Yu et al., 2012). Gene signatures for Hallmark gene sets, biological process GO terms and transcription factor targets were downloaded from the MSigDB database (http://software.broadinstitute.org/gsea/msigdb) using the msigdbr package (Subramanian et al., 2005). Top gene signatures were visualized using built-in functions of clusterProfiler (Wickham, 2009).

QUANTIFICATION AND STATISTICAL ANALYSIS

Statistics and Data Analysis

The weighted mean ploidy was calculated as $\bar{x} = \sum_{i=1}^{n} w_i' x_i$ with w = fraction of cells and x = ploidy state. The relative fold change in weighted mean ploidy was calculated as percentage after 7 days of regeneration based on the weighted mean ploidy before partial hepatectomy. Given a basal weighted mean ploidy of 8 before and a weighted mean ploidy of 12 after regeneration, the relative fold increase is 1.5 or 50 percentage points, respectively (Figure 2B). Depending on the type of data either Student's t-test, one-way or two-way ANOVA with Sidak's or Tukey's multiple comparisons test was used to determine statistical significance. Correlation was

assessed by calculation of Spearman's correlation coefficient (Figure 1F). For comparison of proliferation curves (Figure 2E), nonlinear regression with least-squares-fit was used and curves were compared by the extra sum-of-squared F test. For statistical parameters and significance please refer to the respective figure legends. If not specified otherwise in the figure legend, n represents the number of animals used. The exact number of mice used in the different experiments is shown in Table S7. Generation of graphs and data analysis was performed using Prism 7.00, GraphPad Software.

DATA AND CODE AVAILABILITY

The single-cell whole genome sequencing datasets generated in this study are available at ENA, accession number: PRJEB3254 (https://www.ebi.ac.uk/ena). The corresponding original single cell profile plots for these datasets are available on Mendeley Data (https://data.mendeley.com/datasets/vfpgvhcvh5/1; https://doi.org/10.17632/vfpgvhcvh5.1). ChiP-seq data were generated before and are accessible on the ENCODE project and the GEO database (ENCSR000EVJ; https://www.encodeproject.org/; GSE32673; GSE74006; (https://www.ncbi.nlm.nih.gov/geo/) (Denechaud et al., 2016; Pandit et al., 2012).